J. Fluid Mech. (1991), *vol.* 222, *pp.* 617–646
Printed in Great Britain

Turbulent open-channel flows with variable depth across the channel

By KOJI SHIONO[1] AND DONALD W. KNIGHT[2]

[1] Department of Civil Engineering, University of Bradford, Bradford BD7 1DP, West Yorkshire, UK

[2] School of Civil Engineering, University of Birmingham, Edgbaston, Birmingham B15 2TT, UK

(Received 10 July 1989 and in revised form 21 June 1990)

The flow of water in straight open channels with prismatic complex cross-sections is considered. Lateral distributions of depth-mean velocity and boundary shear stress are derived theoretically for channels of any shape, provided that the boundary geometry can be discretized into linear elements. The analytical model includes the effects of bed-generated turbulence, lateral shear turbulence and secondary flows. Experimental data from the Science and Engineering Research Council (SERC) Flood Channel Facility are used to illustrate the relative importance of these three effects on internal shear stresses. New experimental evidence concerning the spatial distribution of Reynolds stresses τ_{yx} and τ_{zx} is presented for the particular case of compound or two-stage channels. In such channels the vertical distributions of τ_{zx} are shown to be highly nonlinear in the regions of strongest lateral shear and the depth-averaged values of τ_{yx} are shown to be significantly different from the depth mean apparent shear stresses. The importance of secondary flows in the lateral shear layer region is therefore established. The influence of both Reynolds stresses and secondary flows on eddy viscosity values is quantified. A numerical study is undertaken of the lateral distributions of local friction factor and dimensionless eddy viscosity. The results of this study are then used in the analytical model to reproduce lateral distributions of depth-mean velocity and boundary shear stress in a two stage channel. The work will be of interest to engineers engaged in flood channel hydraulics and overbank flow in particular.

1. Introduction

Most natural rivers have flood plains that extend laterally away from the main river channel at a gentle gradient or in a series of terraces. In certain cases multistage channels are deliberately formed in order to increase conveyance capacity in times of flood and to have recreational land available at other times of the year. Two-stage channels thus consist typically of a main river channel in which there is some discharge all of the time and flood plains, which are dry for most of the time yet perform a vital function in times of flood. Since flood alleviation schemes are the focus of much engineering work, the prediction of the conveyance capacity, velocity distribution and boundary shear stress distribution in such channels is clearly important. The boundary shear stress distribution is a prerequisite for studies on bank protection and sediment transport. The prediction of these parameters in two-stage or compound channels is complicated by the lateral exchange of momentum that takes place in the shear layer that forms between the generally faster moving water in the main river channel and the slower moving water on the flood plain.

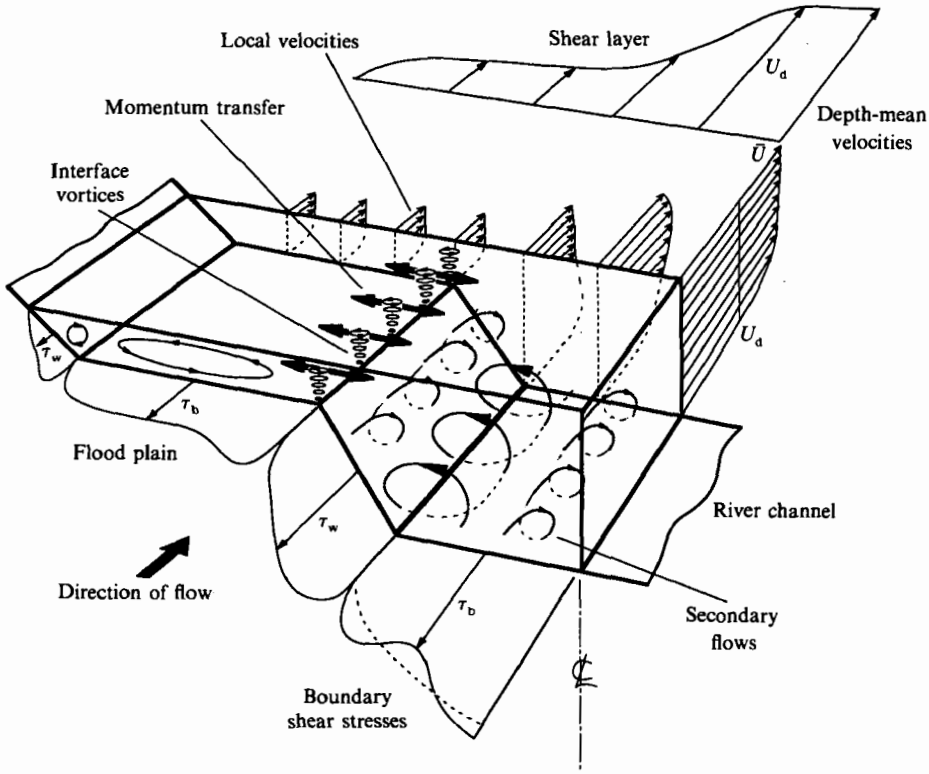

FIGURE 1. Hydraulic parameters associated with overbank flow in a two-stage channel.

The superposition of high lateral shear on bed-generated turbulence and longitudinal secondary flow structures is an intriguing problem in fluid mechanics. In the context of river channels with flood plains, the problem is usually further complicated even for moderately straight channels by the complex geometry of the cross-section and the heterogeneous nature of the boundary roughness. The modelling of such flows is therefore particularly difficult and challenging. Some of the main hydraulic features of overbank flow are shown in figure 1 for a symmetric two-stage channel with a trapezoidal cross-section. A number of one-dimensional empirical formulae, based on apparent shear stresses acting on particular internal interfaces, have been used to predict the stage discharge relationship (H *vs.* Q) for two-stage channels; see for example, Knight & Demetriou (1983), Knight & Hamed (1984), Knight, Demetriou & Hamed (1984), Wormleaton, Allen & Hadjipanos (1982) and Wormleaton & Merrett (1990). Two-dimensional approaches based on depth-averaged parameters have been developed to give the lateral distributions of both velocity and boundary shear stress. These approaches have typically been either numerical, as for example given by Keller & Rodi (1988) and Wormleaton (1988), or analytical, as given by Shiono & Knight (1988). Three-dimensional turbulence models have also been developed and applied to this problem in order to understand the pattern of secondary flow cells and the structure of the shear layer region; see for example Kawahara & Tamai (1988), Krishnappan & Lau (1986) and Larson (1988). However, these three-dimensional models require a large number of empirical constants that make them not very useful for engineering design purposes. The two-dimensional approach therefore seems the best way forward at the moment and

examples of this approach are given by Knight, Shiono & Pirt (1989), Shiono & Knight (1988) and Wormleaton (1988). However, in these three particular examples the secondary flow effects have been ignored, and only lateral shear and bed-generated shear considered.

This paper describes an improved analytical solution, developed from the earlier work of Shiono & Knight (1988), which now includes the effects of secondary flow. Data from the Science and Engineering Research Council Flood Channel Facility (SERC-FCF) are used to quantify the apparent shear stresses across a two-stage channel arising from turbulence and secondary flow effects. These apparent shear stresses are then depth averaged to give dimensionless depth-averaged eddy viscosity values. The analytical solution is thus capable of reproducing the lateral distributions of depth-mean velocity and boundary shear stress in compound or two-stage channels. It has been applied to several natural river channels in the Severn–Trent catchment in order to extend the stage discharge relationship for overbank flow; see Knight *et al.* (1989) and Knight, Samuels & Shiono (1990). A typical symmetric two-stage channel in which there is no crossfall in regions 1 and 3 is shown in figure 2. For a sufficiently wide river channel (region 1) and flood plain (region 3), the depth-averaged velocity, U_d, and boundary shear stress, τ_b, will attain constant but different values in the two regions, thus creating a shear layer in the vicinity of region 2. Owing to the re-entrant and channel corners in this region the flow is also strongly affected by secondary flows.

2. Analytical solution

In order to predict the lateral variation of depth-mean velocity and boundary shear stress in open channel flow, the depth-mean momentum equation has to be solved for steady uniform turbulent flow in the streamwise direction. The equation for the longitudinal streamwise component of momentum on a fluid element may be combined with the continuity equation to give

$$\rho\left[\frac{\partial \bar{U}\bar{V}}{\partial y}+\frac{\partial \bar{U}\bar{W}}{\partial z}\right]=\rho g S_0+\frac{\partial}{\partial y}(-\rho\overline{uv})+\frac{\partial}{\partial z}(-\rho\overline{uw}), \tag{1}$$

where x, y, z are streamwise, lateral and normal directions respectively, $\bar{U}$, $\bar{V}$, $\bar{W}$ are temporal mean velocity components corresponding to x, y, z, u, v, w are turbulent perturbations of velocity with respect to the mean, ρ is the density of water, g is the gravitational acceleration, S_0 is the bed slope gradient ($S_0 = \sin\theta$).

The depth-mean-averaged momentum equation can be obtained by integrating (1) over the water depth, H. Provided $\bar{W}(H) = \bar{W}(0) = 0$, then Shiono & Knight (1988) show that (1) becomes

$$\frac{\partial H(\rho\bar{U}\bar{V})_d}{\partial y}=\rho g H S_0+\frac{\partial H\bar{\tau}_{yx}}{\partial y}-\tau_b\left(1+\frac{1}{s^2}\right)^{\frac{1}{2}}, \tag{2}$$

where τ_b is the bed shear stress, s is the side slope ($1:s$, vertical:horizontal),

$$(\rho\bar{U}\bar{V})_d=\frac{1}{H}\int_0^H \rho\bar{U}\bar{V}\,dz \quad \text{and} \quad \bar{\tau}_{yx}=\frac{1}{H}\int_0^H(-\rho\overline{uv})\,dz.$$

Analytical solutions have been obtained to (2) based on the eddy viscosity approach and by neglecting the secondary flow contribution i.e. ($\partial(H\rho\bar{U}\bar{V})_d/\partial y = 0$). The eddy viscosity approach has been adopted because of its common usage by numerical

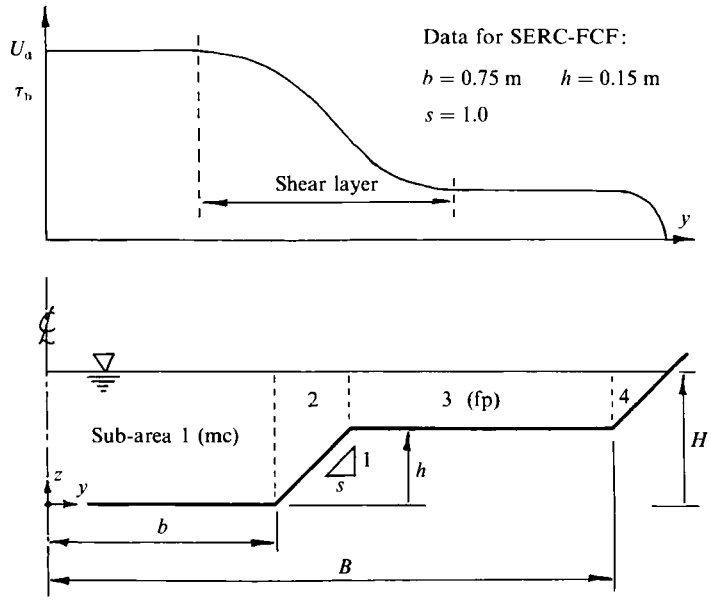

FIGURE 2. Cross-section of a two-stage channel, with notation.

modellers. In this model the depth-averaged transverse shear stress, $\bar{\tau}_{yx}$, is expressed in terms of the lateral gradient of depth-mean velocity

$$\bar{\tau}_{yx} = \rho \bar{\epsilon}_{yx} \frac{\partial U_d}{\partial y}. \tag{3}$$

Since the eddy viscosity has dimensions of $m^2\ s^{-1}$, it is often related to the local shear velocity, U_* and depth, H, by the dimensionless eddy viscosity coefficient, λ, defined by

$$\bar{\epsilon}_{yx} = \lambda U_* H. \tag{4}$$

However as (2) shows, the local shear velocity, U_* $(= (\tau_b/\rho)^{\frac{1}{2}})$ is affected by the free shear layer turbulence and the secondary flows. In regions of high lateral shear it might be argued that the U_* in (4) should be replaced by the primary or shear velocity difference between the two regions. However, in the interests of simplicity and because of its common usage by hydraulic modellers the form of (4) is retained with λ being regarded as a 'catch all' parameter to describe various three-dimensional effects. In order to express (2) in terms of one variable only (U_d or τ_b), the Darcy–Weisbach friction, f $(= 8\tau_b/(\rho U_d^2))$ is used to link U_* and U_d, giving

$$U_* = (\tfrac{1}{8}f)^{\frac{1}{2}} U_d. \tag{5}$$

The depth-averaged eddy viscosity in (4) may then be expressed in the form

$$\bar{\epsilon}_{yx} = \lambda H (\tfrac{1}{8}f)^{\frac{1}{2}} U_d. \tag{6}$$

Substituting (3) and (6) into (2) gives

$$\rho g H S_0 - \tfrac{1}{8}\rho f U_d^2 \left(1 + \frac{1}{s^2}\right)^{\frac{1}{2}} + \frac{\partial}{\partial y}\left\{\rho \lambda H^2 (\tfrac{1}{8}f)^{\frac{1}{2}} U_d \frac{\partial U_d}{\partial y}\right\} = \frac{\partial}{\partial y}\{H(\rho \bar{U}\bar{V})_d\}. \tag{7}$$

In an earlier paper, Shiono & Knight (1988) assumed that $\partial(H\rho\bar{U}\bar{V})_d/\partial y = 0$ and obtained analytical solutions to (7) for channels of various shape. The experimental

results which are described in a later section of this paper suggest that, for the particular cases considered, the shear stress due to secondary flow, $(\rho\bar{U}\bar{V})_{\mathrm{d}}$, decreases approximately linearly either side of a maximum value which occurs at the edge of the flood plain and the main channel. Although this is a first-order approximation to the data, as figure 10 will later show, it does have the merit that it then allows (7) to be solved analytically. Further data from a wider range of channel geometries are clearly needed before this assumption may be generally accepted. However, if this is so, then the lateral gradient of the secondary flow force per unit length of the channel may be written as

$$\frac{\partial(H\rho\bar{U}\bar{V})_{\mathrm{d}}}{\partial y} = \Gamma_{\mathrm{mc}} \quad \text{or} \quad \Gamma_{\mathrm{fp}}, \tag{8}$$

where the subscripts mc and fp refer to the main channel and flood plain respectively. The analytical solution to (7) may then be expressed for a constant-depth, H, domain as

$$U_{\mathrm{d}} = \left\{A_1 \mathrm{e}^{\gamma y} + A_2 \mathrm{e}^{-\gamma y} + \frac{8gS_0 H}{f}(1-\beta)\right\}^{\frac{1}{2}} \tag{9}$$

and for a linear-side-slope domain as

$$U_{\mathrm{d}} = \{A_3 \xi^{\alpha_1} + A_4 \xi^{-\alpha_1 - 1} + \omega\xi + \eta\}^{\frac{1}{2}}, \tag{10}$$

where

$$\left.\begin{aligned} \gamma &= \left(\frac{2}{\lambda}\right)^{\frac{1}{2}}\left(\frac{f}{8}\right)^{\frac{1}{4}}\frac{1}{H}, \quad \beta = \frac{f\Gamma}{8gS_0 H}, \\ \alpha_1 &= -\frac{1}{2} + \frac{1}{2}\left\{1 + \frac{s(1+s^2)^{\frac{1}{2}}}{\lambda}(8f)^{\frac{1}{2}}\right\}^{\frac{1}{2}}, \\ \omega &= \frac{gS_0}{\dfrac{(1+s^2)^{\frac{1}{2}}}{s}\dfrac{f}{8} - \dfrac{\lambda}{s^2}\left(\dfrac{f}{8}\right)^{\frac{1}{2}}}, \\ \eta &= -\frac{\Gamma}{s(1+s^2)^{\frac{1}{2}}\dfrac{2}{\lambda}\left(\dfrac{f}{8}\right)^{\frac{1}{2}}} \end{aligned}\right\} \tag{11}$$

and ξ is the depth function on the side-slope domain (e.g. $\xi = H - ((y-b)/s)$ for the main-channel side slope).

Equations (9)–(11) give the lateral variation of depth-mean velocity and boundary shear stress (via (5)) in a channel of any shape provided that its geometry can be described by a number of linear boundary elements. For a constant-depth domain, (9) shows that as $y \to \infty$ with $\gamma > 0$, since the flow must become two-dimensional ($U_{\mathrm{d}} = \{8gS_0 H/f\}^{\frac{1}{2}}$) in the far field where no secondary flow exists ($\beta = 0$), therefore $A_1 = 0$. For a sloping-side-slope domain, (10) shows that as $s \to \infty$, A_3 must be zero in order that a solution might exist. Equations (9) and(10) also require boundary conditions of continuity of HU_{d} and $\partial(HU_{\mathrm{d}})/\partial y$ across joints of domains, together with the no-slip condition, $U_{\mathrm{d}} = 0$, at the remote boundaries. The subdivision of the channel cross-section into various sub-areas with either constant-depth domains or sloping-side-slope domains will therefore require sufficient computer capacity for the matrix inversion of the coefficients $A_1 \ldots A_n$. Examples of complex natural geometries modelled in this way are given in Knight *et al.* (1989, 1990).

FIGURE 3. General view of a straight two-stage channel moulded in the Science and Engineering Research Council Flood Channel Facility (SERC-FCF) at Hydraulics Research Ltd, Wallingford. (Courtesy of Hydraulics Research Ltd.)

3. Analysis of experimental data

3.1. *Data acquisition*

The SERC Flood Channel Facility (SERC-FCF) consists of a channel 56 m long, 10 m wide with a discharge capacity of 1.1 $m^3 s^{-1}$; see figures 3 and 4. Within the 10 m wide flume a variety of channels can be constructed with different planform geometries (straight, skewed and meandering), different cross-sectional shapes (trapezoidal, idealized natural sections, variable flood plain widths, variable crossfall) and different boundary types (smooth, rough, rigid and loose). The SERC has embarked on an 8 year programme of directed research, the first phase of which, concerning straight and skewed channels, is now coming to a close. During this 3 year period 19 series of experiments have been undertaken, each series corresponding to a particular geometry. This paper concentrates mainly on the data from Series 02, in which a straight two-stage channel was moulded in the facility shown in figures 3 and 4. The geometrical parameters were $B/b = 4.2$, $b/h = 5.0$, $s_1 = s_3 = \infty$, $s_2 = s_4 = 1.0$, $b = 0.75$ m, $h = 0.15$ m, $S_0 = 1.027 \times 10^{-3}$ and $0.15 < H < 0.30$ m, giving $0 < D_r < 0.5$. Both in-bank and out-of-bank experiments were undertaken. The measurement section was 36 m downstream from the inlet to the flume.

The data acquisition system is only described briefly here since full details are given by Elliott & Sellin (1990), Knight & Sellin (1987), Knight & Shiono (1990), Myers & Brennan (1990) and Wormleaton & Merrett (1990). The velocity data were obtained by using multiple 10 mm diameter miniature propeller meters and 60 s time

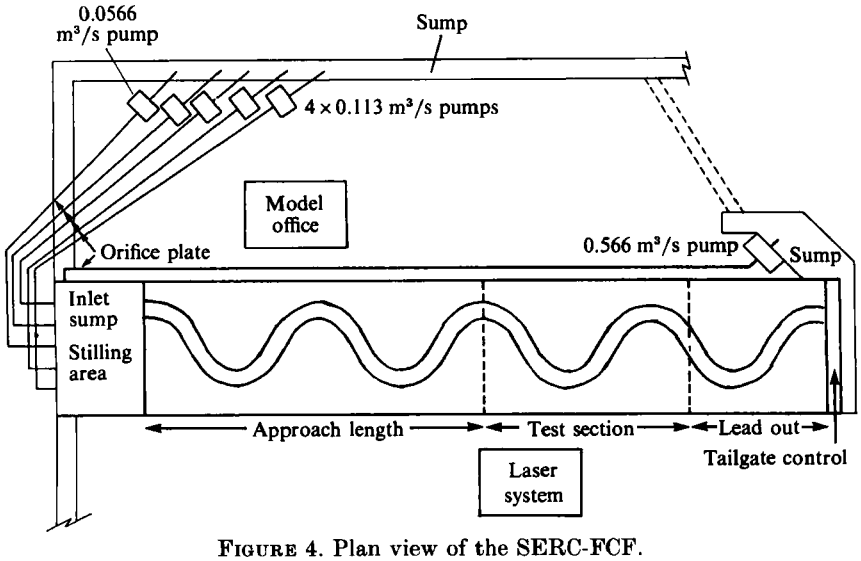

FIGURE 4. Plan view of the SERC-FCF.

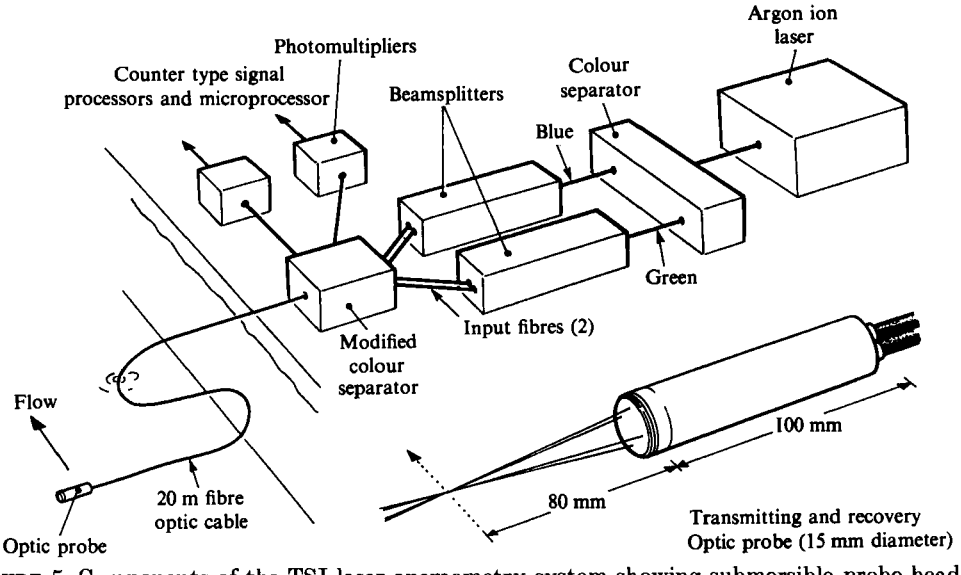

FIGURE 5. Components of the TSI laser anemometry system showing submersible probe head, fibre optic cable, transmitting and receiving optics and processing equipment.

averaging. The boundary shear stresses were measured with 2.7 and 4.0 mm diameter Preston tubes with 50 s time averaging. The turbulence measurements were undertaken with a two-component LDA system (TSI, model 9273), operated in a backscatter mode with a 20 m long fibre-optic cable connecting the laser and processing system to a 15 mm diameter submersible measurement probe; see figure 5.

3.2. *Mean flow parameters*

The main hydraulic features associated with overbank flow are shown in figure 1. In a long reach of a wide river channel the boundary layer will extend over the whole flow depth to give a logarithmic distribution of primary velocity. Where there is a lateral change in depth, as is the case for a two-stage channel, then the depth-mean

velocities will vary laterally creating a transverse shear layer which is superimposed on the bed-generated turbulence. The turbulence generated by the irregular boundaries and the free shear layer are thus responsible for the various secondary flow patterns shown in figure 1. Equation (1) indicates how the gradients of the Reynolds stress components contribute to the secondary flow field. In addition to the longitudinal vortices, a bank of vertical vortices will form in the shear layer along the interface between the main river channel and the flood plain. The flow structures that occur in rivers are therefore extremely complex arising from three distinct physical processes, namely (i) boundary-generated turbulence, (ii) free shear layer turbulence and (iii) velocity fluctuations associated with perturbations in the longitudinal secondary flow cells. Each of these generation mechanisms has its own length and time scales which need to be identified prior to measurement. A frequency analysis of these fluctuations and a detailed discussion of the turbulence data are given by Shiono & Knight (1989) and Knight & Shiono (1990). The resulting boundary shear stress distribution in a two-stage channel is therefore particularly complex, as figure 1 indicates.

3.3. *Reynolds-stress analysis*

The raw data were sampled between 20 and 100 Hz over a period of approximately 60 s at each measurement position within the cross-section. Further details are given by Knight & Shiono (1990). Isometric plots of the Reynolds stresses τ_{yx} and τ_{zx} are shown in figure 6 for four relative depths, D_r, between 0.1 and 0.25 taken from Series 02. The relative depth D_r is the ratio between the depth of flow on the flood plain to that in the main channel, i.e. $D_r = (H-h)/H$. It should be noted that the scales on each diagram vary with the particular value of D_r.

It is clear that for a given value of z, the τ_{yx} values reach a maximum at around $y = 0.9$ m, i.e. at the beginning of the flood plain. Within the lateral shear zone, $0.5 < y < 1.5$ m, the highest values of τ_{yx} are generally near the free surface. At the lowest value of relative depth on which turbulence measurements were possible, i.e. $D_r = 0.1$, the variation of τ_{yx} over the depth is most marked. The depth-mean values, $\bar{\tau}_{yx}$, required in (2) and (3) were therefore obtained by numerical integration of the data for each value of y. Figure 6 also shows that corresponding τ_{zx} values are negative in those places where τ_{yx} values are large. This arises from the force balance in (1). A detailed discussion of the Reynolds stress data is given by Shiono & Knight (1989) and Knight *et al.* (1990), and will not be pursued here, since the main purpose of including one data set here is to illustrate how the depth-mean values $\bar{\tau}_{yx}$, were obtained.

3.4 *Boundary-shear-stress analysis*

The turbulence characteristics of two-dimensional flow in an open channel have been well established by Nezu & Rodi (1986). However, in those cases where the flow is three-dimensional, as is the case with compound channels, then the turbulent structure and boundary shear stress distribution are more complex. See for example Knight & Hamed (1984), Lai & Knight (1988) and Myers & Elsawy (1975). Equation (2) indicates why this is so, and how τ_b differs from the standard two-dimensional value ($\rho g H S_0$) owing to transverse gradients in the additional shear stresses arising from secondary flow and lateral shear effects. Rearranging (2) gives

$$\rho g H S_0 - \tau_b \left(1+\frac{1}{s^2}\right)^{\frac{1}{2}} = \frac{\partial}{\partial y}\{H((\rho \bar{U}\bar{V})_d - \bar{\tau}_{yx})\}. \tag{12}$$

Figure 7 shows some experimental data from the SERC-FCF for three different

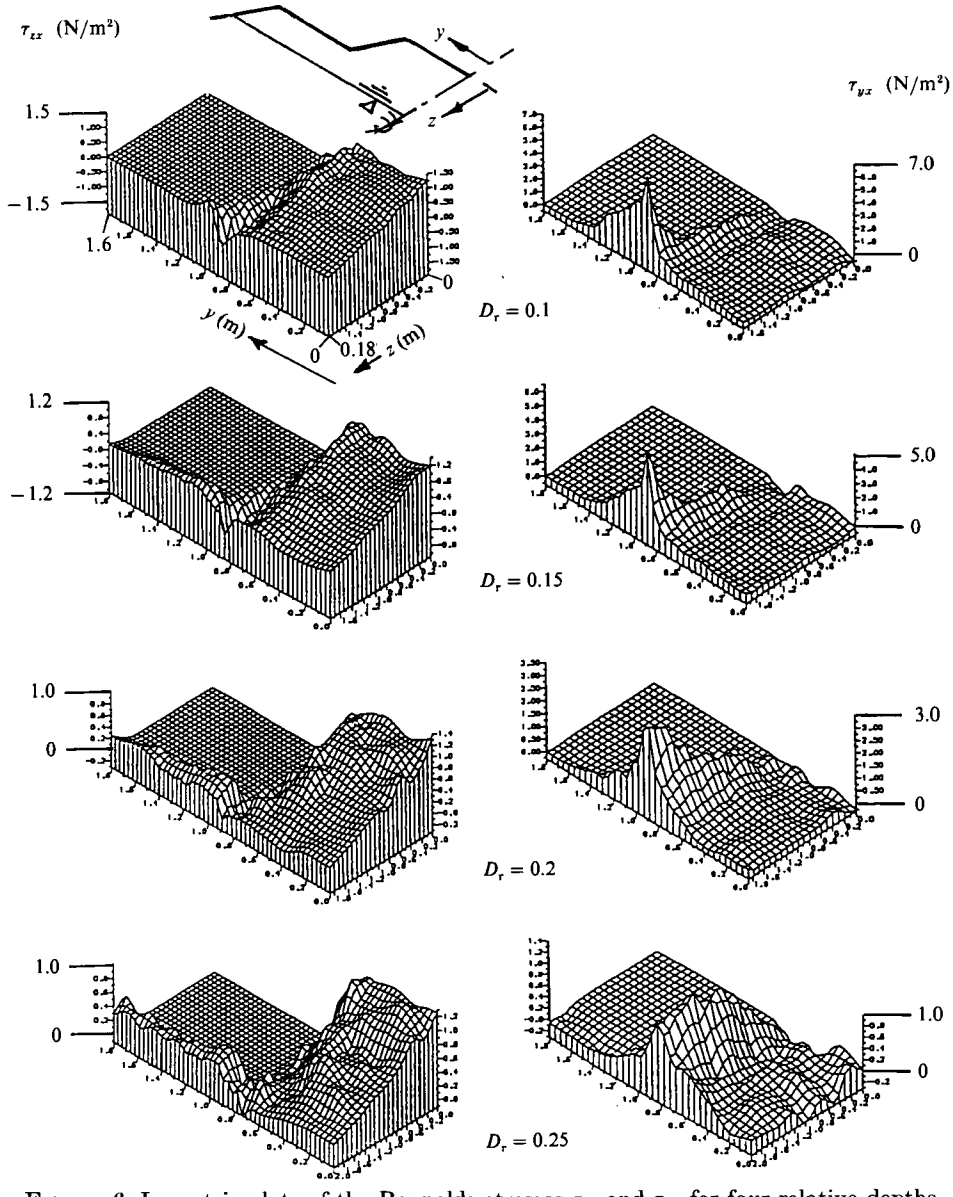

FIGURE 6. Isometric plots of the Reynolds stresses τ_{zz} and τ_{yx} for four relative depths, D_r $(=(H-h)/H)$, in Series 02 with $B/b = 4.2$, $b/h = 5.0$ and $s = 1.0$.

floodplain widths (B/b = 6.67, 4.2 and 2.2, i.e. Series 01–03 respectively), a range of relative depths, D_r = 0.1–0.5 and a main channel side slope s of 1.0. The data have been non-dimensionalized by $\rho g H S_0$. The figure shows that the right-hand side of (12) is non-zero except at two places where $\{H((\rho\bar{U}\bar{V})_d - \bar{\tau}_{yx})\}$ has a local maximum. The gradient of $\{H((\rho\bar{U}\bar{V})_d - \bar{\tau}_{yx})\}$ is clearly positive in the main channel and negative on the flood plain for all B/b values tested. Although the gradient values of $\{H((\rho\bar{U}\bar{V})_d - \bar{\tau}_{yx})\}$ are largely independent of relative depth, D_r, outside the shear layer, the width of the shear layer on the flood plain is strongly dependent upon D_r, increasing as D_r decreases. The same characteristic feature may be noted in the secondary flow results.

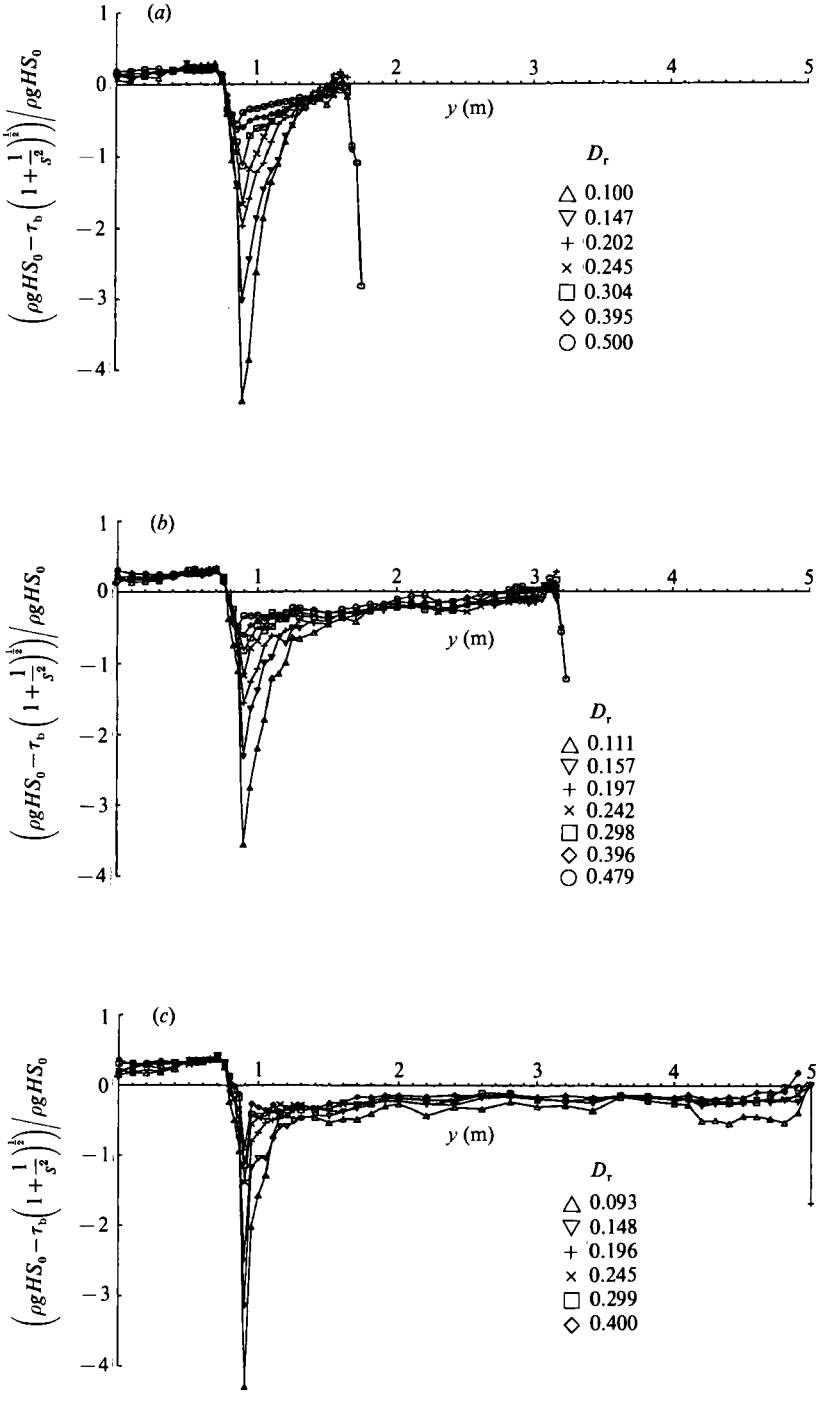

FIGURE 7. Lateral variation of boundary shear stress, τ_b, for different D_r in Series 01–03: (*a*) $B/b = 2.2$, (*b*) 4.2 and (*c*) 6.67 with $b/h = 5.0$ and $s = 1.0$).

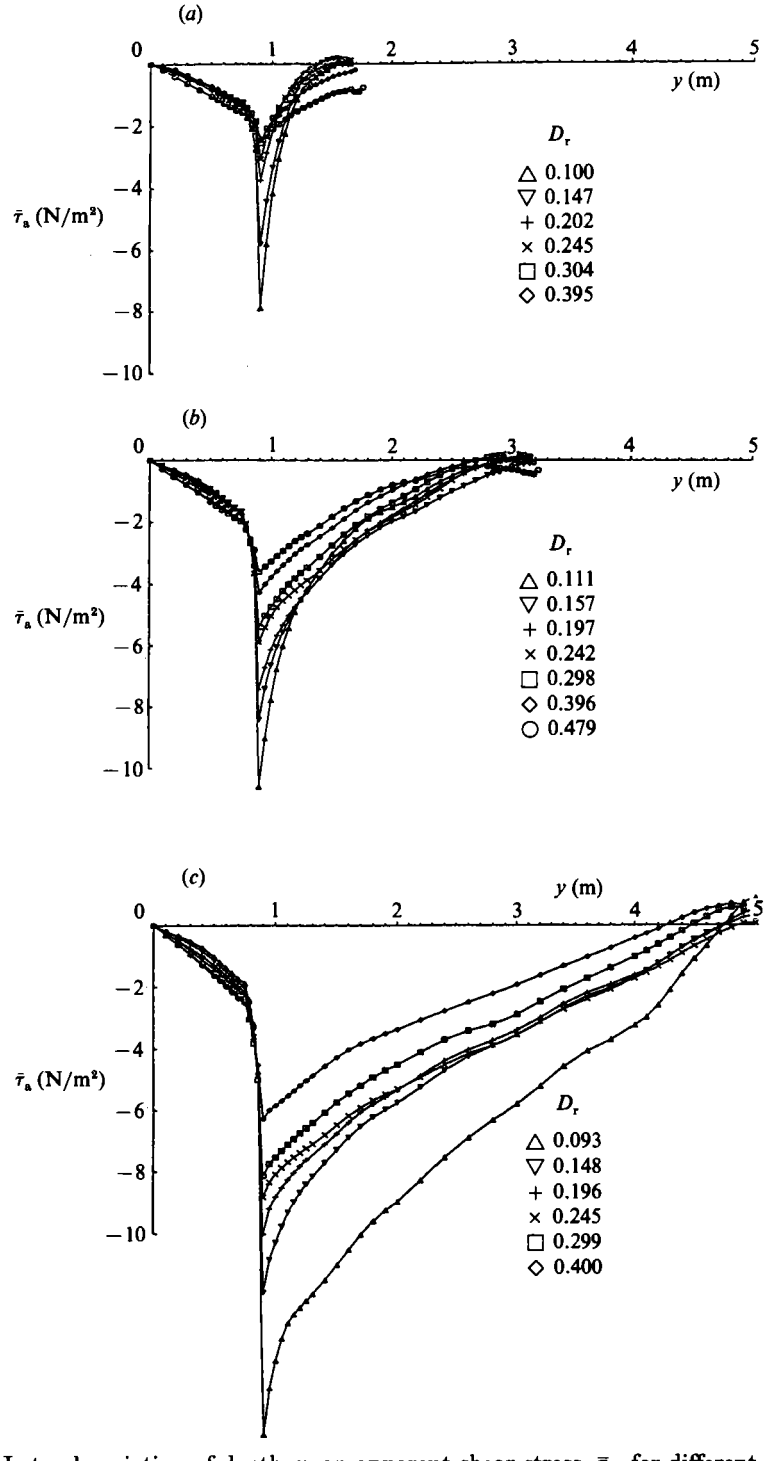

FIGURE 8. Lateral variation of depth-mean apparent shear stress, $\bar{\tau}_a$, for different D_r in Series 01–03, (*a–c*) respectively.

It should be noted that in figure 7 only half the data are shown on account of the symmetry. In general for symmetric cross-sections individual Preston tube and velocity readings were taken on the right-hand side of the system in great detail, and on the left-hand side only at selected points in order to check for flow symmetry. Experience from many other investigations and the SERC-FCF suggested that the flow symmetry was very good. As an overall check, the individual boundary shear stress and velocity readings were integrated laterally (the velocity data having been integrated vertically first), and then compared with the section-mean values obtained independently by water surface slope or orifice measurements. The mean errors for the 23 experiments presented in this paper were -3.1% for τ_b and 0.5% for U. It is interesting to note that despite the strong lateral variations in boundary shear stress the Preston tube calibration of Patel (1965) was found to be remarkably insensitive to the degree of transverse shear imposed in these experiments. This was independently confirmed by the fact that the vertical distributions of Reynolds stress τ_{zx} could be smoothly extrapolated to give bed-shear-stress readings very close to the Preston-tube readings. See Knight & Shiono (1990) and Knight *et al.* (1990) for illustrative plots of this detail. On the basis of these measurements the assumption of symmetry of flow was therefore accepted and $\bar{V}$ was taken as zero at the centreline. This was subsequently also checked by LDA measurements.

The depth-mean apparent shear stress acting on a vertical interface, $\bar{\tau}_a$, may be calculated by integrating (12) to give

$$\bar{\tau}_a = -\frac{1}{H}\int_0^y \left[\rho g H S_0 - \tau_b\left(1+\frac{1}{s^2}\right)^{\frac{1}{2}}\right] \mathrm{d}y. \tag{13}$$

It should be noted that (12) and (13) indicate that this particular apparent shear stress has two quite distinct components, one arising from secondary flows and the other from turbulence. Normally these are lumped together into a single value of $\bar{\tau}_a$ as done by Knight & Demetriou (1983), Myers (1978) and Wormleaton (1988). Values of $\bar{\tau}_a$ based on (13) and the data in figure 7, are shown in figure 8.

It is now possible to quantify the two components in $\bar{\tau}_a$, based on the turbulence data in figure 6. For each value of relative depth, the individual values of τ_{yx} were depth averaged to give the depth-mean values, $\bar{\tau}_{yx}$, which are shown in figure 9. This figure shows that $\bar{\tau}_{yx}$ is approximately zero for $0 < y < 0.6$ m (main channel) and $y > 1.6$ m (flood plain), but that within the lateral shear layer, the values of $\bar{\tau}_{yx}$ rise rapidly and reach a maximum at the beginning of the flood plain ($y = 0.9$ m). As with $\bar{\tau}_a$, the maximum values of $\bar{\tau}_{yx}$ increase and the shear-layer width increases as D_r decreases. However, the relative values of $\bar{\tau}_{yx}$ and $\bar{\tau}_a$ differ throughout the depth range, so that the secondary flow contribution towards $\bar{\tau}_a$ is significant at large relative depths. The second flow contribution was calculated from (12), in the form

$$-(\rho\bar{U}\bar{V})_d = -\frac{1}{H}\int_0^y \left[\rho g H S_0 - \tau_b\left(1+\frac{1}{s^2}\right)^{\frac{1}{2}}\right] \mathrm{d}y - \bar{\tau}_{yx}, \tag{14}$$

using the data in figure 9 for $\bar{\tau}_{yx}$. The results are shown in figure 10, expressed as apparent shear stresses, $(\rho\bar{U}\bar{V})_d$, and apparent shear forces per unit length, $H(\rho\bar{U}\bar{V})_d$.

Figure 10 shows the maximum value of $(\rho\bar{U}\bar{V})_d$ again occurs at $y = 0.9$ m, i.e. at the edge of the flood plain, and that it decreases almost linearly with y for all relative depths. This may indicate that there is just one large secondary flow cell on the flood plain, except near the far corner region. In the main channel the decrease in $(\rho\bar{U}\bar{V})_d$ is again virtually linear for $y < 0.6$ m. However, in the corner of the main channel ($0.6 < y < 0.75$ m) and on the main channel side slope ($0.75 < y < 0.9$ m) the distribution

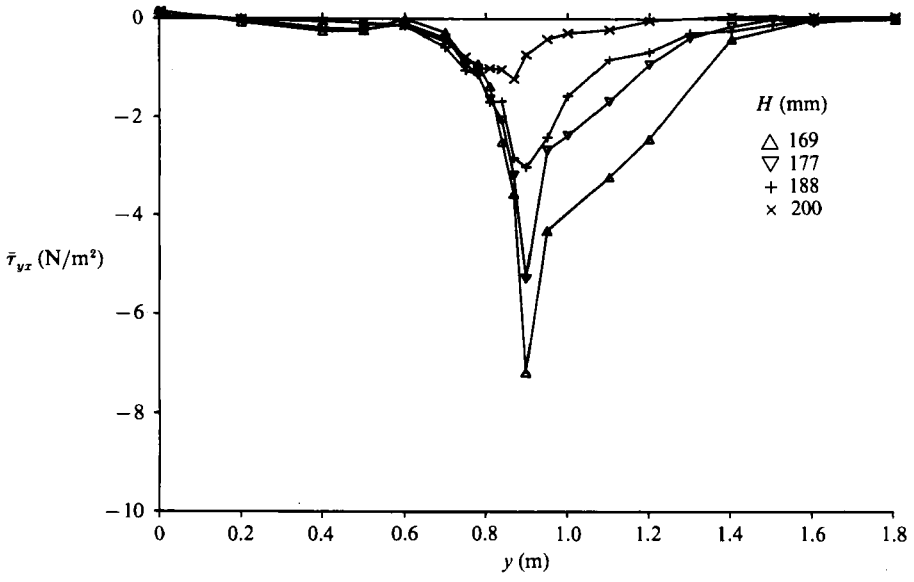

FIGURE 9. Lateral variation of depth-averaged Reynolds stress, $\bar{\tau}_{yx}$, for H = 169–200 mm in Series 02.

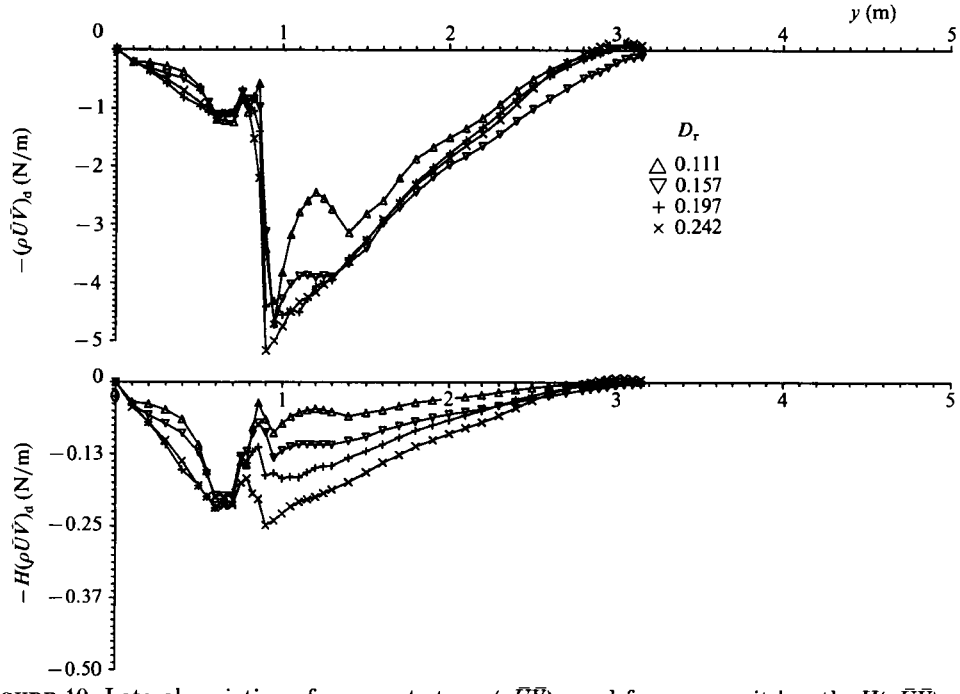

FIGURE 10. Lateral variation of apparent stress $(\rho\bar{U}\bar{V})_d$, and force per unit length, $H(\rho\bar{U}\bar{V})_d$, due to secondary flows for different D_r in Series 02.

is more complex, possibly indicating the presence of a number of secondary flow cells. The perceived linear variations of $(\rho\bar{U}\bar{V})_d$ with y outside this corner region are the basis of the assumption behind (8).

An attempt was made to measure the secondary flow structures with the LDA system and some results are shown in figure 11. Also shown in figure 11 (*a*)–(*d*) are the

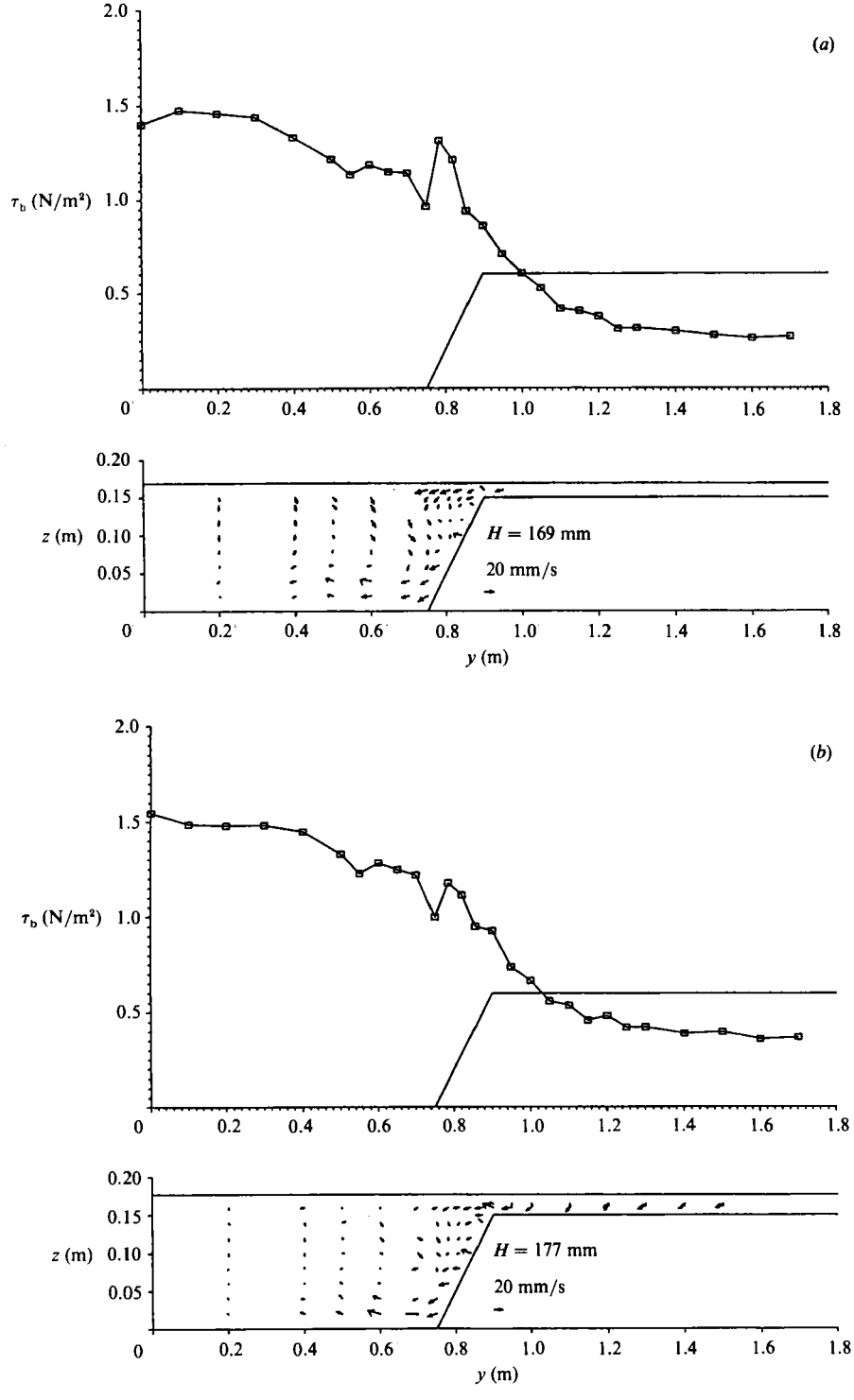

FIGURE 11 (*a*, *b*). For caption see facing page.

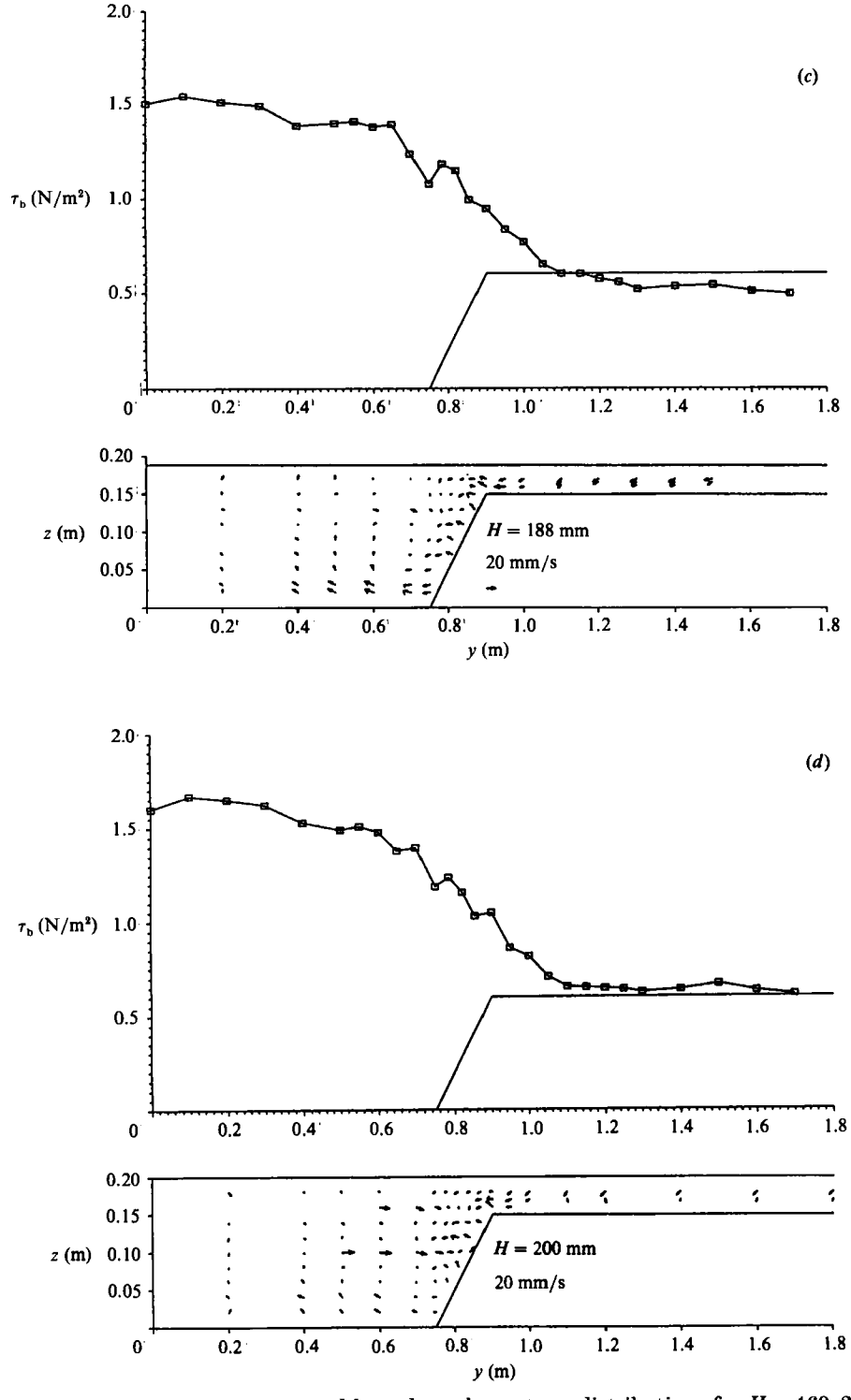

FIGURE 11. Secondary flow vectors and boundary shear stress distributions for H = 169–200 mm in Series 02. (*a*) $D_r = 0.1$, (*b*) 0.15, (*c*) 0.2, (*d*) 0.25.

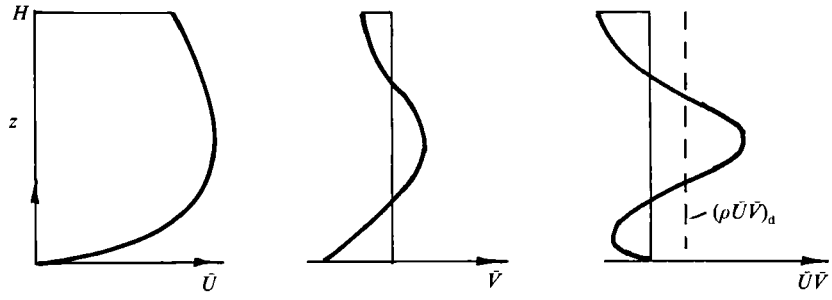

(*a*) Main channel, $y = 0.7$ m

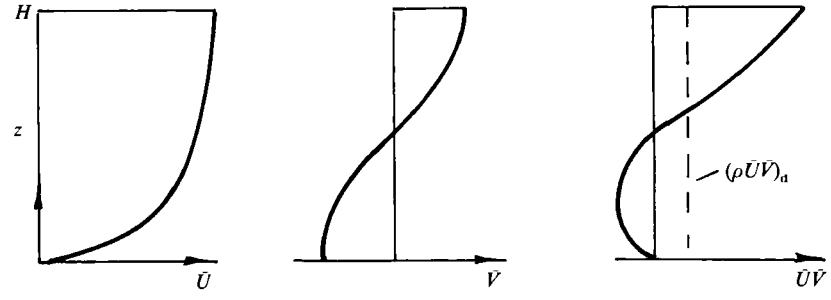

(*b*) Flood plain, $y = 1.2$ m

FIGURE 12. Vertical distributions of primary and transverse mean velocities, $\bar{U}$ and $\bar{V}$, together with $\bar{U}\bar{V}$ and $(\rho\bar{U}\bar{V})_d$.

lateral distributions of boundary shear stress, τ_b, obtained from the Preston tube readings. It should be noted that the vertical scale in figure 11 has been exaggerated 2:1. The data again correspond to Series 02 ($B/b = 4.2, s = 1.0$) for $D_r = 0.1, 0.15, 0.2$ and 0.25. The values of $\bar{V}$ were recalculated from the raw data using a frame rotation of $-2°$ in order to make $\bar{V} = 0$ at the centre of the main channel ($y = 0$). The values of $\bar{W}$ were adjusted by $+1°$ in order to give $\bar{W} = 0$ near the bed at the centreline ($y = 0, z = 0.02$ m). These adjustments were made in this early series of experiments since the LDA probe measuring head was not perfectly aligned. In subsequent experiments very little rotational correction was needed. However, even in those cases where great care was exercised, it was not possible to measure the left-hand side of (14) directly, since for $\bar{U} = 0.6$ m s^{-1} and $(\rho\bar{U}\bar{V})_d = 2$ N/m^2, i.e. typical values, $\bar{V}$ would be 3.3 mm s^{-1}, requiring a rotational accuracy of less than 0.3°. It therefore follows that the only effective way of determining values of $(\rho\bar{U}\bar{V})_d$ is by direct measurements of the lateral distributions of τ_b and τ_{yx} and the application of (14). To the authors' knowledge figure 10 represents one of the few data sets available for $(\rho\bar{U}\bar{V})_d$ for this type of channel flow. Errors in the Reynolds stress measurements due to a 1° error in frame rotation were calculated to be at worst 4% (~ 0.08 N/m^2) and at best less than 1% (~ 0.016 N/m^2).

The secondary flow results in figure 11 show that there are two major secondary flow cells in the vicinity of the main channel side slope. These cause a strong upflow towards the main channel from the re-entrant corner at the edge of the flood plain,

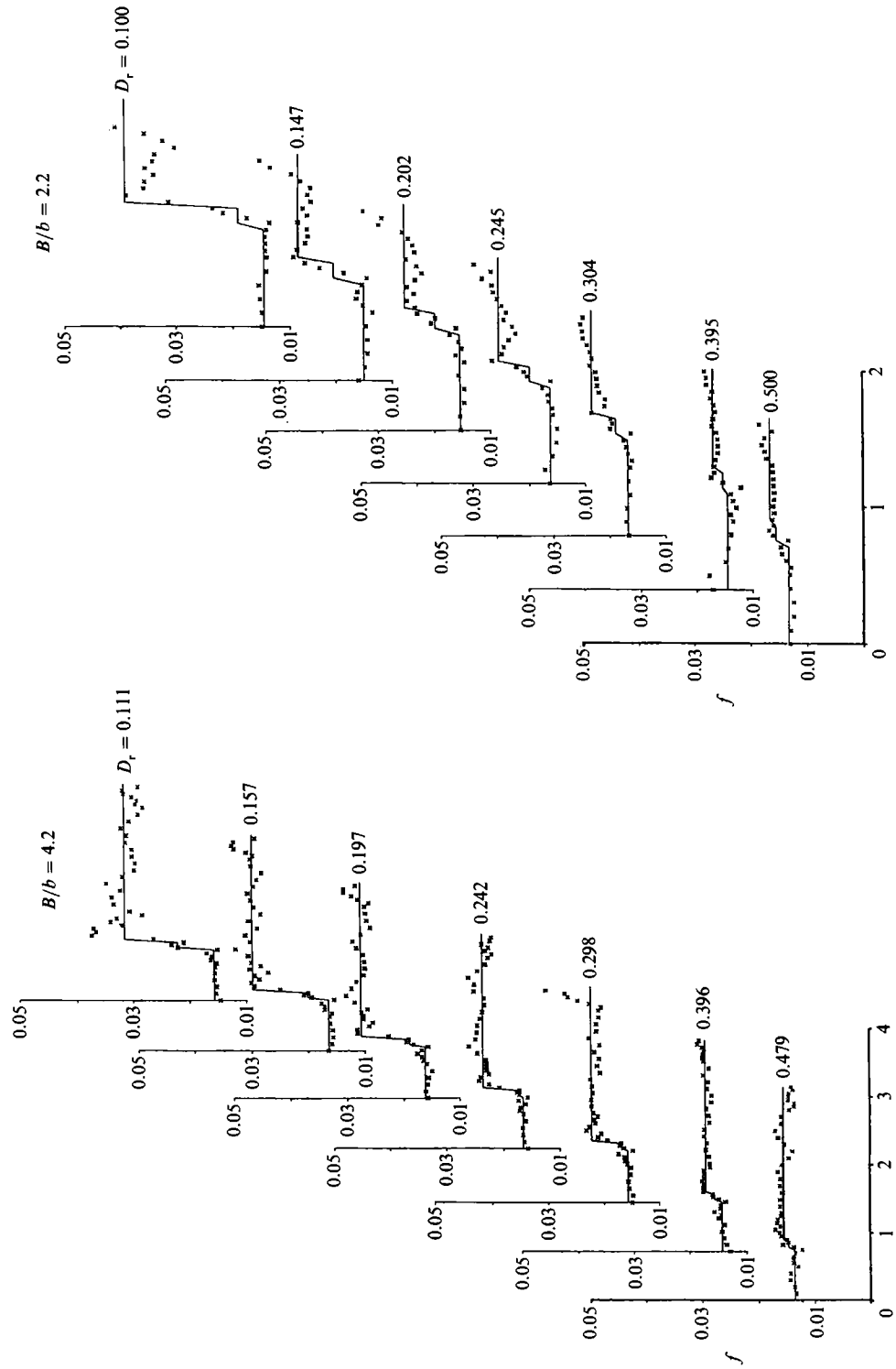

FIGURE 13. Lateral variation of local friction factor, $f\,(=8\tau_b/(\rho U_d^2))$ for various D_r in Series 02 and 03 ($B/b = 4.2$ and 2.2 respectively).

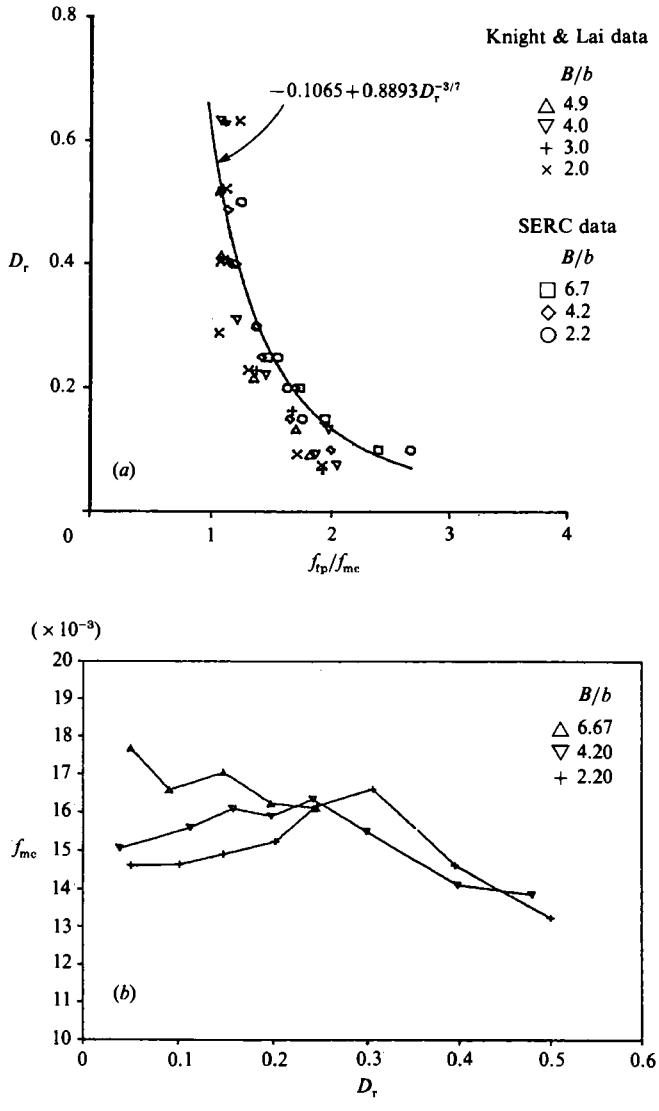

FIGURE 14. (*a*) Variation of the ratio of the friction factors of the flood plain and the main channel, f_{fp}/f_{mc}, with D_r. (*b*) Variation of the main channel friction factor, f_{mc}, with D_r.

and a corresponding downflow in the corner of the main channel. These structures can be seen for a range of side slopes in Shiono & Knight (1989). The effect of these secondary flows on the vertical distributions of horizontal velocity is shown in figure 12. The depth-mean values of $(\rho\bar{U}\bar{V})$ are shown to be always positive, a feature consistent with the earlier results shown in figure 10.

3.5. *Friction-factor analysis*

In order to be able to apply (9)–(11) effectively, the distribution of local friction factor f across the section needs to be known. Experimentally determined values of $f(= 8\tau_b/(\rho U_d^2))$, based on Preston tube and velocity data are shown in figure 13 for Series 02 and 03, with $B/b = 4.2$ and 2.2 respectively. For each series the relative

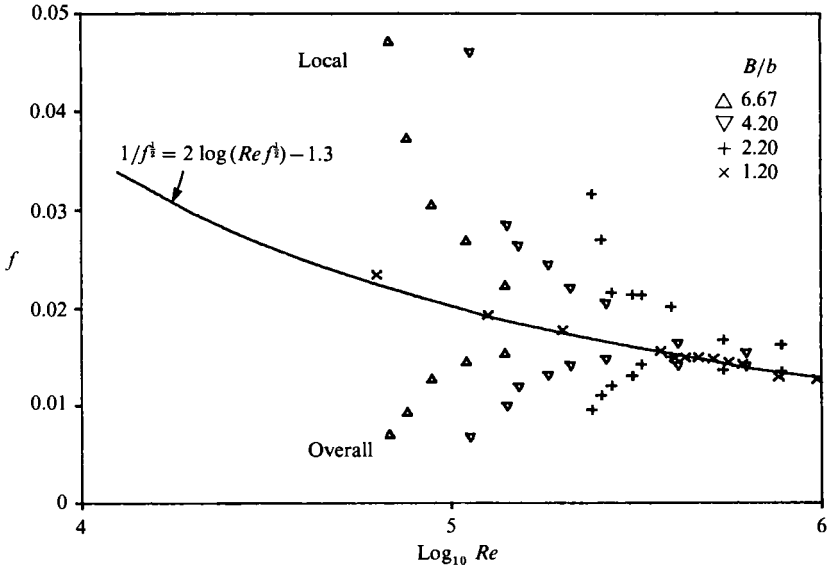

FIGURE 15. Variation of the overall and local friction factors with Reynolds number, $Re = 4U_0R/\nu$, for two-stage channels (Series 01–04).

depth D_r was varied from 0.1 to 0.5. The figure indicates that the friction factor f is sensibly constant in the main channel and on the flood plain except for remote regions of the flood plain for $B/b = 2.2$ and low D_r. The solid lines in figure 13 are the averaged values in the main channel, side slope and flood plain sub-areas. In general the friction factor on the flood plain, f_{fp}, increases relative to the friction factor in the main channel, f_{mc}, as D_r decreases. This would be expected on the grounds of the difference between the Reynolds number in each sub-area. According to the Blasius equation for smooth surfaces, $f \propto Re^{-\frac{1}{4}}$, and therefore the ratio f_{fp}/f_{mc} will depend upon $D_r^{-\frac{3}{7}}$. Figure 14(*a*) shows this to be true for the SERC-FCF data where the best-fit line gives

$$f_{fp}/f_{mc} = -0.1065 + 0.8893 D_r^{-\frac{3}{7}}. \tag{15}$$

Also shown in figure 14(*a*) are the data of Knight & Lai (1986), obtained from wind tunnel experiments. These data also illustrate the increase in f_{fp}/f_{mc} as D_r decreases. The variation of f_{mc} with B/b and D_r is given in figure 14(*b*).

The relationship between the one-dimensional overall friction factor, f_0, and the overall Reynolds number, Re, is often used in compound channel flow analysis, see for example Myers & Brennan (1990). Data from the SERC-FCF are shown in figure 15, in which the one-dimensional friction factor, f_0 ($= 8gRS_0/U_0^2$, where R is the hydraulic radius, U_0 the section-mean velocity) and the local averaged friction factor, f_a ($= (1/P)\int f\,dy$, where P is the wetted perimeter) are both plotted against the overall Reynolds number ($= 4U_0R/\nu$). Figure 15 shows that for overbank flow with a given B/b, f_0 values are below the standard smooth curve of Prandtl and decrease with decreasing Reynolds number, whereas f_a values are above the standard smooth curve and increase with decreasing Reynolds number. This arises because f_0 is strongly influenced by the sudden decrease in hydraulic radius, R, as the flow goes out of the bank (corresponding to a sudden increase in wetted perimeter P for little change in area, A). Conversely f_a is influenced by the relatively large values of the friction factor on the flood plain. It therefore follows that care needs to be exercised

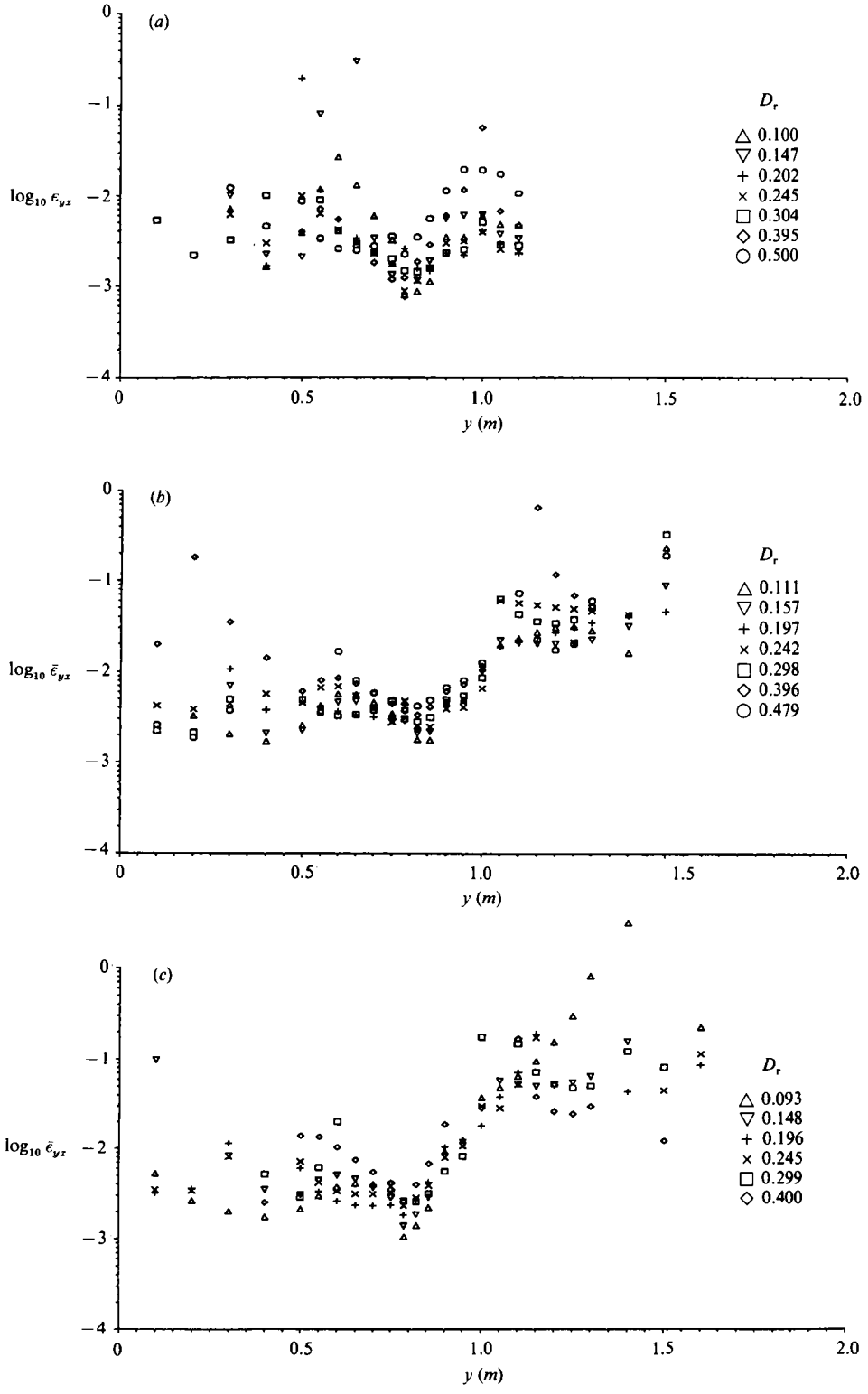

FIGURE 16. Lateral variation of depth averaged transverse eddy viscosity, $\bar{\epsilon}_{yx}$ ($m^2 s^{-1}$) for various D_r in Series 01–03. (*a*) $B/b = 2.2$, (*b*) 4.2 (*c*) 6.6.

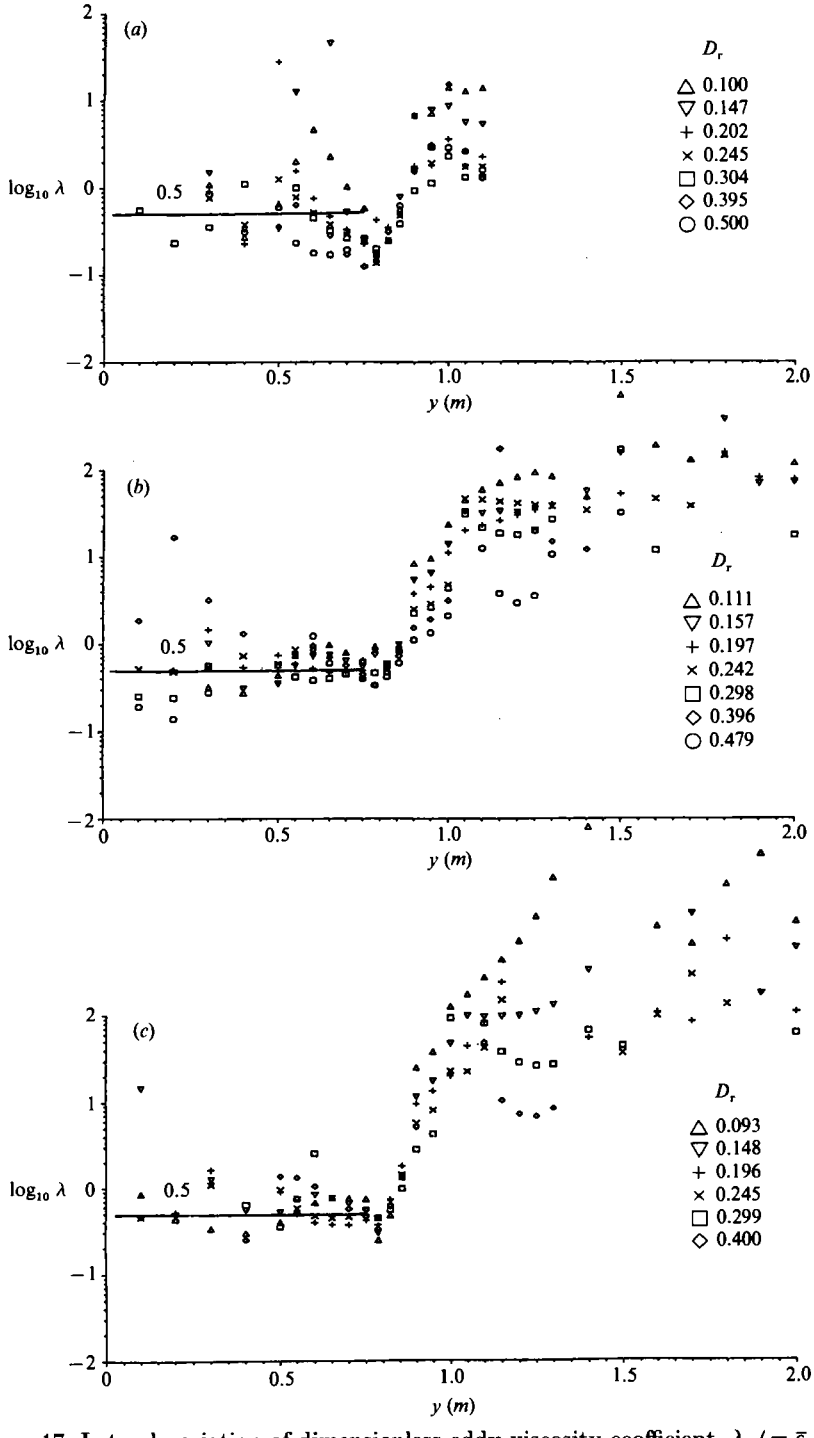

FIGURE 17. Lateral variation of dimensionless eddy viscosity coefficient, λ, $(= \bar{\epsilon}_{yz}/(U_* H))$ for various D_r in Series 01–03.

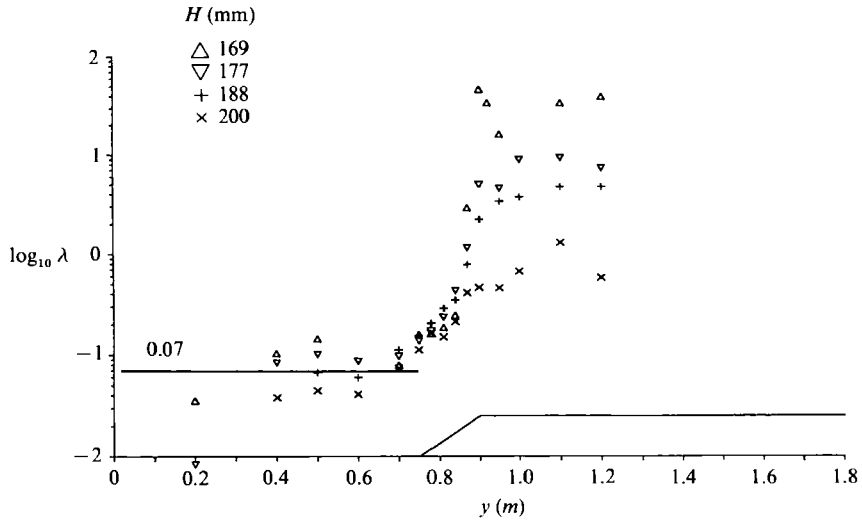

FIGURE 18. Lateral variation of dimensionless eddy viscosity, λ, based on turbulent stresses alone for various depths, H, in Series 02 ($B/b = 4.2$).

before using standard friction factor versus Reynolds number equations in estimating the conveyance capacity of compound channels.

3.6. *Eddy-viscosity analysis*

The depth-mean apparent shear stresses, defined by (13) and shown in figure 8, were used to determine the depth-averaged eddy viscosities, $\bar{\epsilon}_a (= \bar{\tau}_a/(\rho \partial U_d/\partial y))$ and dimensionless eddy-viscosity coefficients, $\lambda_a (= \bar{\epsilon}_a/(U_* H)$. These are shown in figures 16 and 17 for the three cases $B/b = 2.2$, 4.2 and 6.67, all with $s = 1.0$. The local velocity gradient, $\partial U_d/\partial y$, was estimated by a third-order polynomial best fit to five consecutive data points. Considerable scatter in the processed data will result from this procedure where the gradients are small, i.e. for $y > 1.5$ m in the $B/b = 6.67$ case.

Figure 16 shows that the minimum values of eddy viscosity occur on the main channel side slope ($0.75 < y < 0.9$ m). The values tend to increase on the flood plain, with the degree of increase being related to the B/b value. The dimensionless eddy-viscosity values, λ_a, in figure 17 also show an increase with increasing B/b on the flood plain, but also indicate a dependence upon the relative depth, D_r. The λ_a values in the main channel are more or less constant at about 0.5 for all B/b and D_r values tested.

Figure 18 shows the corresponding dimensionless eddy viscosity values based on the turbulence data in figure 9 for $B/b = 4.2$. In the main channel $\lambda \approx 0.07$ for all D_r, which corresponds closely to the standard depth-averaged two-dimensional value for open channel flow ($\lambda = 0.067$). As with figure 17, figure 18 also shows that λ values increase on the flood plain, the degree of increase being related to the value of the relative depth, D_r. Figure 19 shows that the relationship between the flood plain and main channel values may be expressed by

$$\lambda_{fp}/\lambda_{mc} = (2D_r)^{-4}, \tag{16}$$

where $\lambda_{mc} = 0.07$. This relationship is only valid within the range tested, i.e. $0.1 < D_r < 0.25$. Further turbulence data are required to check the form of (16) for other

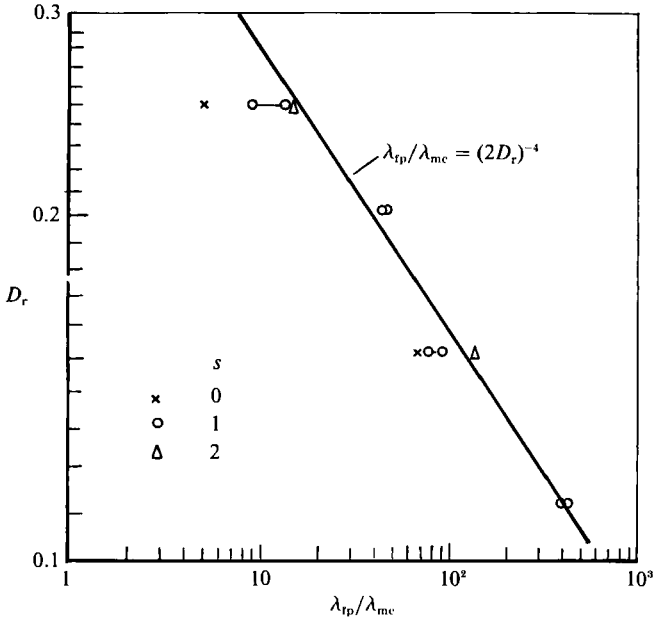

FIGURE 19. Variation of the ratio between the flood plain and main channel dimensionless eddy-viscosity values, $\lambda_{fp}/\lambda_{mc}$, with D_r and side slope s.

geometries. The results presented in figures 17 and 18 indicate that the λ values in the main channel, which include secondary flow effects, are of the order of 10 times larger than those based solely on turbulence.

4. Application of the analytical model

The analytical model described earlier has been applied to a number of channels (Shiono & Knight 1988) with the assumption that the secondary flow term in (7) is small, i.e. $\Gamma = 0$. In these cases the local-averaged friction factor f_a was used in order to calculate the depth-mean velocity, and good agreement between the analytical model results and the data was obtained. It is now known that f_a is higher than the main channel averaged friction factor and lower than the flood plain averaged value. Since the friction factor f is combined with the Γ-factor via β through (9) and (11), this means that secondary flow effects can be included by enhancing the sub-area values of f. Although this will lead to correct distributions of depth-mean velocity, U_d, the values of the boundary shear stress τ_b, will be in error for those cases where secondary flow effects are important. For wide channels and natural rivers these effects may be small and an example of how the analytical model can be calibrated against field data is given by Knight *et al.* (1989, 1990).

In those cases where secondary flows are important then an appropriate value for Γ (or β) has to be chosen for each sub-area. Figure 10 has already shown that the effect of secondary flows on $\bar{\tau}_a$ is approximately linear in all regions except in the vicinity of the main channel side slope ($0.75 < y < 0.9$ m). In this region there is both a positive and a negative gradient in $(\rho\bar{U}\bar{V})_d$. It is therefore suggested that this region be divided into two smaller sub-areas with appropriate β-coefficients. Where greater precision is required the number of sub-areas can of course be increased.

Figure 20 shows the application of the analytical model to one series of SERC-FCF

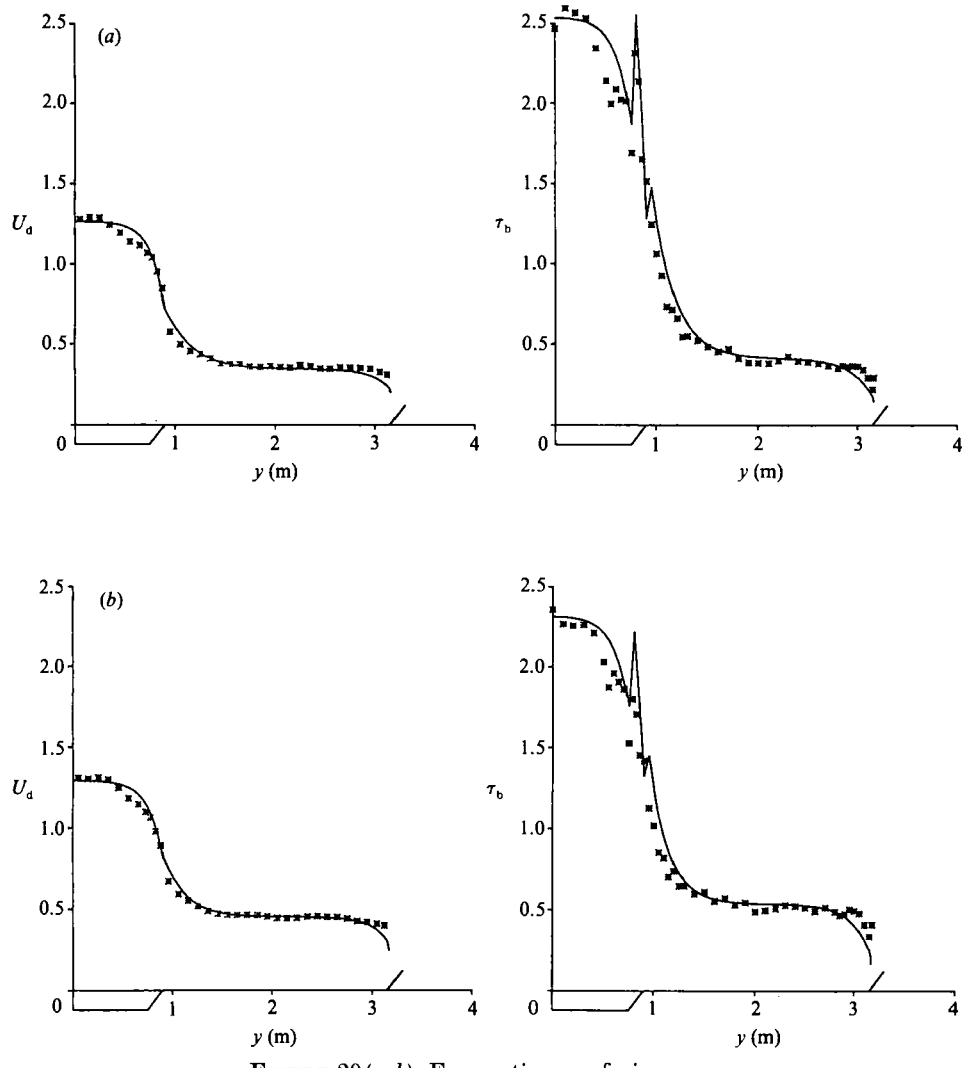

FIGURE 20(*a*, *b*). For caption see facing page.

data (Series 02 with $B/b = 4.2$) and how (9) and (10) model the lateral distributions of U_d and τ_b over a wide range of depths. For these predictions, Γ was taken as zero in sub-areas 2 and 4 (using the notation in figure 2), with $\lambda_1 = 0.07$, $\lambda_2 = \lambda_4 = 0.16$ and $\lambda_3 = 0.07(2D_r)^{-4}$, based on (16). The corresponding friction factors were taken as follows: f_1 values from figure 14(*b*), f_3 values from (15), $f_2 = \frac{1}{2}(f_1 + f_3)$ and $f_4 = f_3$. For sub-areas 1 and 3, Γ-values were calculated from a linear approximation to figure 10, giving $\Gamma_1/(\rho g H S_0) = 0.15$ and $\Gamma_3/(\rho g(H-h)S_0) = -0.25$.

The results shown in figure 20 indicate that the analytical model is capable of predicting the lateral distributions of U_d and τ_b in the presence of strong lateral shear. There is generally quite good agreement between the analytical and experimental values, although the analytical model appears to overestimate both U_d and τ_b around $y = 0.5$ m at the shallowest depths ($D_r = 0.2$ and 0.15), possibly owing to complex structure to the flow in this region. However, given that λ and f values were taken as constant over four large sub-areas, and that the Γ values were first-order

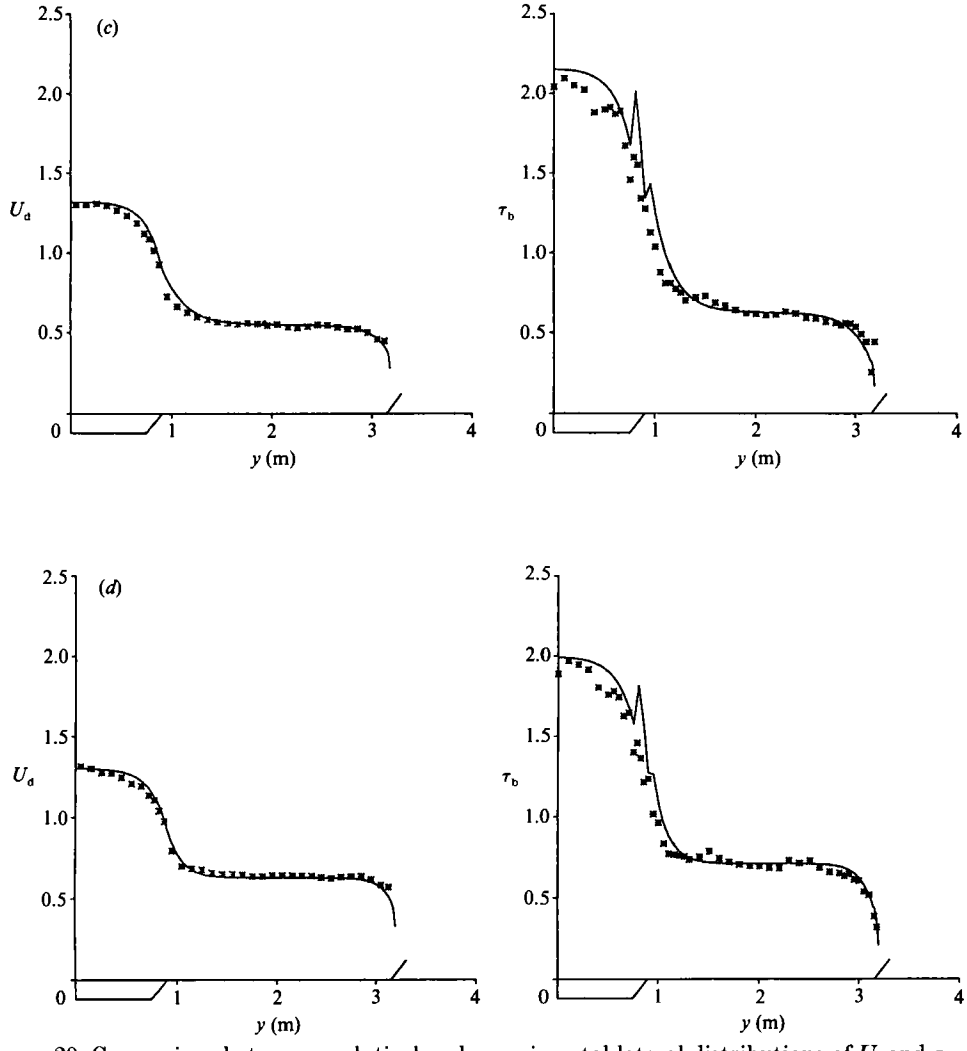

FIGURE 20. Comparison between analytical and experimental lateral distributions of U_d and τ_b, for various D_r in Series 02. (*a*) $D_r = 0.111$, (*b*) 0.157, (*c*) 0.197, (*d*) 0.242. ——, Analytical solution; *, data.

approximations to figure 10 and completely ignored in sub-areas 2 and 4, the predictions are surprisingly good. Further refinement could be undertaken using smaller sub-areas in the vicinity of the edge of the flood plain. For practical engineering purposes, however, the lateral distributions of U_d and τ_b are probably as accurate as they need to be and may be used for predicting either the stage discharge relationship (by lateral integration of U_d) or the sediment transport rate (by use of local τ_b values and a transport equation). An attempt at applying the model to natural river geometries with 7 or 11 sub-areas has been made with a view to predicting the stage discharge curve for overbank flows. Some results are given for three gauging stations in the Severn–Trent catchment by Knight *et al.* (1989, 1990). In each case the channel was much more complex than that modelled in the SERC-FCF and there were considerable variations in roughness around the wetted perimeter. The variation of λ and f in each sub-area with stage appeared to be

reasonably systematic, enabling the lateral distribution of velocity to be estimated for extreme flood events. These were subsequently laterally integrated to produce stage discharge curves.

5. Discussion

The analytical model described above involves those depth-averaged parameters that are likely to be of the most practical use to engineers engaged in flood alleviation schemes. The lateral distributions of depth-averaged velocity in a river form the basis of flow measurement by the current meter method. Lateral integration of the individual readings gives not only the total discharge for a given water level or stage, but also, and more importantly in multistage channels, the proportion of flow occurring in different sub-areas of the channel. Theoretical predictions of U_d for given stage, geometry and roughness conditions are therefore useful inputs to both these aspects of river gauging. An accurate description of the lateral distribution of boundary shear stress in open channel flow is also important in many sediment transport theories or calculation methods through the use of the local shear velocity, $U_* = (\tau_b/\rho)^{\frac{1}{2}}$, in sediment transport equations; see for example Ackers & White (1973) and Garde & Ranga Raju (1977). Furthermore, turbulence simulation models have tended to concentrate on the flow field rather than on τ_b, arising from the sensitivity and difficulty of applying wall functions in strongly sheared layers or where secondary flows are important; see Nakayama, Chow & Sharma (1983), Naot & Rodi (1982) and Younis & Abdellatif (1989). The analytical predictions shown in figure 20, based on an understanding of the lateral distributions of local friction factors in figures 13–15, appear to offer the practising engineer a sufficiently accurate description of U_d and τ_b for two-stage channels without recourse to three-dimensional modelling. The experimental data from the SERC-FCF have provided sufficient detail of the various three-dimensional flow structures for the particular problem of overbank flow to enable them to be incorporated into this two-dimensional analytical model.

Use of the eddy-viscosity model may be criticized on the grounds of its simplicity. However, its use in open channel flow calculations is likely to persist into the foreseeable future for two reasons: Firstly the topographically complex geometry, the heterogeneous nature of the boundary roughness and the uncertainty in being able to prescribe boundary roughness coefficients sufficiently accurately for natural river channels and flood plains makes a more refined calculation method not only inappropriate but also difficult to calibrate successfully for natural flows. Secondly, and arising from the first, is that for estuaries and rivers, in which two-stage or multistage channels commonly exist, engineering calculation methods must of necessity average parameters over a large area in a grid representation of the flow physics. It therefore follows that in certain types of model, depth-averaged stresses $\bar{\tau}_{yx}$ or $\bar{\tau}_{xy}$ on vertical sections, or area-averaged bottom shear stresses τ_b within designated areas will still be the basic parameters adjusted in any calibration procedure. The experimental results shown in figure 6 indicate clearly some of the implications of depth averaging on the Reynolds stresses and on the three-dimensional flow structures that occur when bed-generated turbulence, lateral shear turbulence and secondary flows interact on the section of a channel where the transverse variations in depth are large. The depth-mean turbulent stresses $\bar{\tau}_{yx}$, shown in figure 9 and the depth-mean apparent stresses, $\bar{\tau}_a$ shown in figure 8 need to be understood in the context of the full three-dimensional picture shown in figure 6.

The highly nonlinear nature of the Reynolds stresses on a horizontal plane, τ_{zx}, which are analysed in detail by Shiono & Knight (1989), Knight & Shiono (1990) and Knight *et al.* (1990), point to the complexity of the flow.

Given that eddy-viscosity models are still appropriate for many types of engineering calculation, then one of the more significant experimental results to come from the SERC-FCF is the relative contributions of $(\rho\bar{U}\bar{V})_d$ and $\bar{\tau}_{yx}$ to $\bar{\tau}_a$, illustrated in figures 8–11. It is clear that for channels with small lateral crossfall, the secondary-flow-induced stresses make a significant contribution to the total apparent shear stress used in engineering design. For two-stage channels the secondary flows also greatly extend the lateral shear layer width on the flood plain. Having also demonstrated the considerable experimental difficulties in measuring $(\rho\bar{U}\bar{V})_d$ directly, and the need to determine it indirectly via (12) and (13) and detailed measurements of τ_b and τ_{yx}, it follows that field studies of lateral dispersion coefficients may require some further study. Published reviews by Lau & Krishnappan (1977) and Nokes & Wood (1987, 1988) all indicate λ-values of around 0.134 for f-values greater than 0.055, regardless of the aspect ratio of the channel. Although these two reviews acknowledge that λ is a catch-all type of parameter, it must clearly be made up of at least two components, and the present results may assist in identifying them.

The experimental data on $\bar{\epsilon}$ or λ in figures 16 and 17 should be of interest to modellers simulating real flows in natural rivers. Although the scale of the SERC-FCF is still relatively modest, the flume is an order of magnitude larger than many flumes in university hydraulics laboratories. The practical difficulties of measuring τ_b sufficiently accurately in the field under flood flow conditions, together with the time taken to measure τ_{yx} values, mean that the SERC-FCF data will remain one of the few sources of information concerning the relative importance of the various terms in (14). The relative contributions of turbulence and secondary flows to λ-values, as shown in figures 17 and 18, are therefore significant and need to be appreciated by those using numerical models.

Figure 20 shows that the analytical model is capable of predicting the lateral distributions of U_d and τ_b in a two-stage channel to a high degree of accuracy. This is not altogether surprising in this instance since the experimental data were used to develop two key coefficients in the model. These were the values of Γ (figure 10) and f (figures 14 and 15). The f-values are however corroborated to a certain degree by other data (14*a*), as well as theoretical reasoning. Further experimental evidence is therefore urgently required before the analytical model can be used without recourse to individual calibration for each type of channel. Notwithstanding this, the model can be used for novel geometries and heterogeneous roughness conditions since the calibration is relatively straightforward using known distributions of U_d data; see for example Knight *et al.* (1989).

6. Conclusions

(i) An improved analytical model is given for steady, uniform, turbulent flow in a compound or two-stage channel. The analytical model gives the lateral distributions of depth-mean velocity, U_d, and boundary shear stress, τ_b, for prismatic channels and includes the effects of bed-generated turbulence, lateral shear turbulence and secondary flows.

(ii) The depth averaging of parameters, which is required to reduce an essentially three-dimensional problem to a two-dimensional one capable of solution, does not appear to have significantly reduced the predictive capability of the analytical

model. However, there are very large spatial variations in the Reynolds stresses in the region of highest lateral shear that require further analysis.

(iii) The conventional depth-averaged apparent shear stress, $\bar{\tau}_a$, is shown to be composed of two elements, one due to turbulence, $\bar{\tau}_{yx}$, and the other due to secondary flows $(\rho\bar{U}\bar{V})_d$. The only realistic way of determining $(\rho\bar{U}\bar{V})_d$ has been shown to be via (14), which requires detailed measurements of boundary shear stresses and Reynolds stresses. The relative strength of $(\rho\bar{U}\bar{V})_d$, and its influence on the lateral spreading of the shear layer, have been shown to be independent of the relative depth, D_r $(= (H-h)/H)$.

(iv) In two-stage channels the local friction factors, $f(= 8\tau_b/(\rho U_d^2))$ are approximately constant, but different, in the main channel and flood plain regions. The ratio between the flood plain and main channel friction factors increases as the relative depth decreases, in accordance with the variation of local Reynolds number, i.e. $f_{fp}/f_{mc} \propto D_r^{-\frac{3}{7}}$.

(v) Dimensionless eddy-viscosity values, λ, have been obtained from both apparent shear stresses, $\bar{\tau}_a$, and depth-averaged Reynolds stresses, $\bar{\tau}_{yx}$. In the context of overbank flow there is almost an order of magnitude difference between them. In the main channel, λ_a values are around 0.5, whereas λ-values based on turbulence alone are around 0.07. The λ and λ_a values will increase exponentially on the side-slope domain and attain constant but larger values on the flood plain. The ratio between the flood plain and main channel dimensionless eddy-viscosity values based on turbulence alone is shown to be depth dependent and given by $\lambda_{fp}/\lambda_{mc} = (2D_r)^{-4}$.

(iv) The analytical predictions of U_d and τ_b in two-stage channels are shown to be in close agreement with the experimental data from the SERC Flood Channel Facility.

The authors gratefully acknowledge the financial and technical support of the Science & Engineering Research Council and Hydraulics Research Limited. They are particularly grateful to members of the SERC Steering Group in Hydraulics, Pollution Control and Public Health Engineering who encouraged the development of this national facility. Some further financial support from six of the UK Regional Water Authorities and the Ministry of Agriculture, Fisheries and Food, is also acknowledged. Finally the authors would like to thank the many members of the SERC Working Party on Flood Channels, both academic and industrial, for the many stimulating discussions and comments about the research programme.

REFERENCES

Ackers, P. & White, W. R. 1973 Sediment transport: new approach and analysis. *J. Hydraul. Div. ASCE* **99**, (HY11), pp. 2041–2060.

Elliott, S. C. A. & Sellin, R. H. J. 1990 SERC Flood Channel Facility: Skewed flow experiments. *J. Hydraul. Res.* **28**, 197–214.

Garde, R. J. & Ranga Raju, K. G. 1977 *Mechanics of Sediment Transportation and Alluvial Stream Problems*. New Delhi: Wiley Eastern.

Kawahara, H. & Tamai, N. 1988 Numerical calculations of turbulent flows in compound channel with an algebraic stress turbulence model. *Proc. 3rd Intl Symp. on Refined Flow Modelling and Turbulence Measurements, Tokyo, Japan, July*, pp. 9–17.

Keller, R. J. & Rodi, W. 1988 Prediction of flow characteristics in main channel flood plain flows. *J. Hydraul. Res.* **26**, 425–441.

Knight, D. W. & Demetriou, J. D. 1983 Flood plain and main channel flow interaction. *J. Hydraul. Engng ASCE* **109**, 1073–1092.

KNIGHT, D. W., DEMETRIOU, J. D. & HAMED, M. E. 1984 Stage discharge relationships for compound channels. *Proc. 1st Intl Conf. on Channels and Channel Control Structures* (ed. K. V. H. Smith), pp. 4.21–4.35. Springer.

KNIGHT, D. W. & HAMED, M. E. 1984 Boundary shear in symmetrical compound channels. *J. Hydraul. Engng ASCE* **110**, 1412–1430.

KNIGHT, D. W. & LAI, C. J. 1986 Compound duct flow data, vol. 10. *University of Birmingham, Dept. of Civil Engng Rep.* pp. 1–73.

KNIGHT, D. W., SAMUELS, P. G. & SHIONO, K. 1990 River flow simulation: research and developments. *J. Inst. Water Environ. Management* **4**, pp. 163–175.

KNIGHT, D. W. & SELLIN, R. H. J. 1987 The SERC Flood Channel Facility. *J. Int. Water Environ. Management* **1**, 198–204.

KNIGHT, D. W. & SHIONO, K. 1990 Turbulence measurements in a shear layer region of a compound channel. *J. Hydraul. Res.* **28**, 175–196.

KNIGHT, D. W., SHIONO, K. & PIRT, J. 1989 Prediction of depth mean velocity and discharge in natural rivers with overbank flow. *Intl Conf. Hydraulic and Environmental Modelling of Coastal, Estuarine and River Waters, Bradford University, England* (ed R. A. Falconer, P. Goodwin & G. S. Matthew), pp. 419–428. Gower Technical Press.

KRISHNAPPAN, B. G. & LAU, Y. L. 1986 Turbulence modelling of flood plain flows. *J. Hydraul. Engng, ASCE* **112**, 251–266.

LAI, C. J. & KNIGHT, D. W. 1988 Distributions of streamwise velocity and boundary shear stress in compound ducts. *Proc. 3rd Intl Symp. on Refined Flow Modelling and Turbulence Measurements, Tokyo, Japan, July*, pp. 527–536.

LARSON, R. 1988 Numerical simulation of flow in compound channels. *Proc. 3rd Intl Symp. on Refined Flow Modelling and Turbulence Measurements, Tokyo, Japan, July*, pp. 527–536.

LAU, L. & KRISHNAPPAN, B. G. 1977 Transverse dispersion in rectangular channels. *J. Hydraul. Div. ASCE* **103** (HY10), 1173–1189.

MYERS, R. C. & ELSAWY, E. M. 1975 Boundary shear in channel with flood plain. *J. Hydraul. Engng, ASCE* **7**, 933–947.

MYERS, W. R. C. 1978 Momentum transfer in a compound channel. *J. Hydraul. Res.* **16**, 139–150.

MYERS, W. R. C. & BRENNAN, E. K. 1990 Flow resistance in compound channels. *J. Hydraul. Res.* **28**, 141–155.

NAKAYAMA, A., CHOW, W. L. & SHARMA, D. 1983 Calculation of fully developed turbulent flows in ducts of arbitrary cross-section. *J. Fluid Mech.* **128**, 199–217.

NAOT, D. & RODI, W. 1982 Calculation of secondary currents in channel flow. *J. Hydraul. Div. ASCE* **108** (HY8), 948–968.

NEZU, I. & RODI, W. 1986 Open channel flow measurements with a laser doppler anemometer. *J. Hydraul. Engng, ASCE* **112**, 335–355.

NOKES, R. I. & WOOD, I. R. 1987 Lateral turbulent dispersion in open channel flow. *Proc. 22nd Biennial Congress, IAHR, Lausanne*, pp. 233–338.

NOKES, R. I. & WOOD, I. R. 1988 Vertical and lateral turbulent dispersion: some experimental results. *J. Fluid Mech.* **187**, 373–394.

PATEL, V. C. 1965 Calibration of the Preston tube and limitations on its use in pressure gradients. *J. Fluid Mech.* **23**, 185–195.

SHIONO, K. & KNIGHT, D. W. 1988 Two dimensional analytical solution for a compound channel. *Proc. 3rd Intl Symp. on Refined Flow Modelling and Turbulence Measurements, Tokyo, Japan, July* (ed. Y. Iwasa, N. Tamai & A. Wada), pp. 503–510.

SHIONO, K. & KNIGHT, D. W. 1989 Vertical and transverse measurements of Reynolds stress in a shear region of a compound channel. *Proc. 7th Intl Symp. on Turbulent Shear Flows, Stanford, USA, August*, pp. 28.1.1–28.1.6.

WORMLEATON, P. R. 1988 Determination of discharge in compound channels using the dynamic equation for lateral velocity distribution. *Proc. Intl Conf. on Fluvial Hydraulics, Budapest.*

WORMLEATON, P. R., ALLEN, J. & HADJIPANOS, P. 1982 Discharge assessment in compound channel flow. *J. Hydraul. Div. ASCE* **108** (HY9), 975–993.

WORMLEATON, P. R. & MERRETT, D. 1990 An improved method of calculation for steady uniform flow in prismatic main channel/flood plain sections. *J. Hydraul. Res.* **28**, 157–174.

YOUNIS, B. A. & ABDELLATIF, O. E. 1989 Modelling of sediment transport in rectangular ducts with a two-equation model of turbulence. *Proc. Intl Symp. on Sediment Transport Modelling, ASCE, New Orleans, August*, pp. 197–202.